

<https://doi.org/10.1038/s44264-026-00127-y>

# Multiobjective spatial optimization of fertilizer rates enables sustainable crop production in southwest China

Guitang Liao<sup>1</sup> ✉, Jianmin Qian<sup>2</sup>, Peng He<sup>3</sup>, Zhengyu Lin<sup>3</sup>, Tianfei Dai<sup>4</sup>, Gang He<sup>5</sup>, Chenghua Xu<sup>1</sup> & Xi Gou<sup>2</sup> ✉

Achieving the dual goals of ensuring food security and environmental security is a global challenge in sustainable nutrient management. However, previous studies have neglected the spatialization of nutrient management. Here, we proposed a new approach to assess and optimize fertilizer rates by combining data-driven forecasting and machine learning methods to address spatially optimal allocation of nutrient resources. We found that the contribution of fertilizer application to crop yields in Southwest China decreased by 1–3% from 2009 to 2019. Crop nutrients were widely unbalanced, with obvious nitrogen excess, local phosphorus deficiency, and general potassium deficiency, while plains and riverbanks were hotspots of nutrient excess. Multiobjective optimization reduced the nitrogen fertilizer rate by 18% ( $11 \times 10^4$  t) with a slight increase in the crop yield, whereas the ratio of nitrogen, phosphorus, and potassium fertilizers was optimally adjusted from 1:0.38:0.33 to 1:0.51:0.42, conforming with national expectations.

Food security is a critical sustainable development goal<sup>1</sup>. However, the resource and environmental costs associated with food production have become prohibitively high in recent decades<sup>2</sup>. Excessive nitrogen and phosphorus inputs to more than half of the world's crops<sup>3</sup>, coupled with a generally low fertilizer use efficiency<sup>4</sup>, have resulted in farmland greenhouse gas emissions<sup>5</sup>, surface water pollution<sup>6</sup>, and biodiversity loss<sup>7</sup> that exceed the planet's environmental boundaries<sup>8</sup>. It is estimated that in global food systems, the nitrogen and phosphorus use efficiency must be doubled to meet both food security and ecological safety goals<sup>9,10</sup>. How to feed the projected<sup>9</sup> billion people in the future while avoiding ecosystem collapse has become a major challenge for ensuring global sustainability<sup>11,12</sup>. Optimizing the cropland layout<sup>13,14</sup> and transforming crop allocation<sup>15,16</sup> can mitigate the negative environmental impacts of food production, but socioeconomic and cultural barriers still hinder the implementation of these strategies<sup>17</sup>. Therefore, the precise allocation and regulation of farmland nutrient resources are particularly important for achieving the goal of zero hunger under planetary boundary constraints<sup>18–20</sup>.

The precise management of farmland nutrients has remained a challenge for digital agriculture because of the complex relationships among crops, soils, fertilizers and other environmental factors<sup>21</sup>. Three key issues must be addressed: the first issue is accurate crop yield prediction, which is a prerequisite for nutrient demand assessment. Over the years, meteorological

models<sup>22</sup>, remote sensing models<sup>23</sup> and crop growth models<sup>24</sup> have been widely employed for crop yield prediction. Meteorological models are mainly used to assess the impact of climate change on the crop yield because of the single predictor variable adopted<sup>25,26</sup>. Remote sensing models can be used to quickly and accurately predict crop yields at large scales by modeling the relationships between multispectral data (Thematic Mapper (TM), Moderate Resolution Imaging Spectroradiometer (MODIS), and photosynthetically active radiation (FPAR) data) or agronomic parameters (normalized difference vegetation index (NDVI), enhanced vegetation index (EVI), leaf area index (LAI), and net primary production (NPP)) and observed yields<sup>27,28</sup>, but they can hardly explain yield changes<sup>23</sup>. Crop growth models, such as the decision support system for agrotechnology transfer (DSSAT)<sup>29</sup>, WORld FOod STudies (WOFOST) model<sup>30</sup>, CropGrow<sup>31</sup>, and Agricultural Production Systems Simulator (APSIM)<sup>32</sup>, aim to simulate the crop growth process and provide accurate yield predictions (the prediction errors are generally smaller than 10%). However, owing to the complexity and heterogeneity in ecosystems, it is difficult to obtain many parameters for crop growth models<sup>24</sup>. Currently, new models that combine multisource environmental data (meteorological, soil, topographic, crop and management, and other data)<sup>33–36</sup> with machine learning algorithms (artificial neural network (ANN), random forest (RF), support vector machine (SVM), long short-term memory (LSTM), etc.)<sup>37–41</sup> have become the frontier

<sup>1</sup>College of Resources and Environment, Chengdu University of Information Technology, Chengdu, China. <sup>2</sup>General Station of Arable Soil Quality and Fertilizer of Sichuan Province, Chengdu, China. <sup>3</sup>Agricultural Information and Rural Economy Research Institute, Sichuan Academy of Agricultural Sciences, Chengdu, China. <sup>4</sup>Sichuan Green Food Development Center, Chengdu, China. <sup>5</sup>Yibin Agricultural Comprehensive Service Center, Yibin, China.

✉ e-mail: [liaoqutang1982@163.com](mailto:liaoqutang1982@163.com); [13730638373@163.com](mailto:13730638373@163.com)

and hotspot of crop yield prediction<sup>42</sup>. In particular, the RF algorithm, which not only accurately captures the complex nonlinear relationship between the crop yield and environmental factors but also provides the importance of predictor variables, has broad application prospects in crop yield prediction<sup>43,44</sup>.

The second issue is the accurate assessment of nutrient balances, which is key to identifying the location and degree of crop nutrient deficiencies or excesses<sup>45</sup>. Scholars have assessed global<sup>46,47</sup>, national<sup>48–51</sup>, and regional<sup>52–54</sup> nutrient balances by comparing nutrient inputs and outputs of agroecosystems<sup>55,56</sup> or soil systems<sup>57,58</sup>. However, as crop yields and nutrient inputs have mostly been derived from statistical panel data, many studies can reflect only the overall nutrient balances within administrative districts or ecological zones, but it is difficult to achieve spatially accurate assessment and mapping of nutrient balances for different crops at different scales<sup>59,60</sup>. In recent years, field-localized experiments and observations have provided the basis for accurate calculations of crop nutrient balances. Unfortunately, owing to the high geographical variation in crop nutrient balances, reliable methods for upscaling fertilizer field experiment data at the macroscopic scale remain lacking<sup>61,62</sup>. Therefore, the accurate calculation and mapping of crop nutrient balances, driven by large amounts of data on soils, fertilizers, crops and other environmental factors, has become an important trend in sustainable nutrient management in farmland<sup>63,64</sup>.

The third issue is the precise regulation of farmland nutrients. Soil management zoning has long been an important approach for achieving precision fertilization<sup>65</sup>. Scholars have selected soil, meteorological, topographic and other indicators for comprehensive evaluation to delineate fertilizer management units with relatively consistent natural conditions to achieve spatially precise quantification of fertilizer inputs under specific target yields<sup>66–70</sup>. In recent years, quantitative research on the fertilizer reduction potential has become a hotspot for nutrient regulation. Most previous studies were based on soil monitoring and fertilizer field experiments, thereby comparing the recommended fertilizer rates with the actual fertilizer rates employed by farmers<sup>71,72</sup> or comparing the soil nutrient content with environmental thresholds<sup>73,74</sup> to estimate nutrient excess or deficiency areas. Unfortunately, these studies are highly compartmentalized. On the one hand, precision fertilization and fertilizer reduction are considered two separate topics, and the spatial redistribution and balancing of farmland nutrients have not been systematically addressed. On the other hand, food security and ecological security objectives have been addressed separately, thereby neglecting their consistency. Farmland nutrient regulation entails a multiobjective optimization problem, and the trade-offs and coordination between food production and environmental pressures must be considered<sup>75,76</sup>. The nondominated sorting genetic algorithm (NSGA) is currently one of the most representative multiobjective optimization algorithms<sup>77</sup> and has been widely applied in land use optimization<sup>78</sup>, crop structure adjustment<sup>79</sup> and ecological protection planning<sup>80</sup>, which has provided new opportunities for multiobjective farmland nutrient optimization management.

Over the next 30 years, China's food production not only faces the risk of yield stagnation in one-third of the region<sup>81</sup> but also exhibits the need to

reduce phosphorus and nitrogen losses, greenhouse gas emissions, and blue water depletion by more than half to meet the national environmental security boundary<sup>82</sup>. In particular, major grain-producing regions have become the center of agricultural nonpoint source pollution in China, and there is an urgent need to improve the sustainable management of farmland nutrients<sup>83,84</sup>. For this reason, many soil monitoring<sup>85</sup>, fertilization surveys<sup>86,87</sup> and fertilizer experiments<sup>88,89</sup> have been conducted in China over the past 20 years, which has significantly contributed to soil nutrient assessment and fertilizer formulation development<sup>90</sup>. However, relevant studies and applications are isolated and fragmented<sup>91</sup> and generally lack effective methods for spatially mining and modeling big data on soil nutrients, fertilizer inputs and crop yields, making it difficult to meet the systematic and precise requirements for future nutrient management decisions<sup>21,92</sup>. Therefore, adopting a major grain-producing region in Southwest China as an example, a multiobjective farmland nutrient optimization method was proposed that integrates multisource big data and intelligent optimization algorithms to achieve (1) accurate prediction of crop yield distributions under different nutrient conditions; (2) accurate assessment of the crop nutrient balance; and (3) spatial optimization of crop fertilizer rates under the dual objectives of ensuring food security and ecological security.

## Results

### Spatial heterogeneity in the contribution of fertilizer application to the crop yield

Six RF-based yield prediction models were established in ArcGIS for the three crops considered (Tables 1, 2 and Supplementary Fig. 1), which were generally well fitted and reliable, with R<sup>2</sup> values above 0.89, mean absolute error (MAE) values between 0.56 and 0.9 t ha<sup>-1</sup>, root mean square error (RMSE) values ranging from 0.8 to 1.21 t ha<sup>-1</sup>, and symmetric mean absolute percentage error (SMAPE) values between 10.02 and 24.46%. Moreover, the prediction accuracy of the rice RF model was greater than that of the maize and wheat RF models, which may be related to the larger number of training samples for the rice model. In particular, the prediction accuracy for the fertilized yield (YF) was significantly greater than that for the soil-based yield (YS), with the SMAPE of the YF prediction model ranging from 10.02 to 15.24%, whereas that of the YS prediction model ranged from 14.52 to 24.46%. This phenomenon reflects, on the one hand, that the YS exhibits greater uncertainty and is determined by more complex influencing factors and, on the other hand, that fertilization increases the predictability for the crop yield.

From 2009 to 2019, crop yields in the study area showed an increasing trend (Figs. 1 and 2). The soil-based yield (YS) is the crop yield in the current year without fertilization, reflecting the inherent soil productivity of farmland<sup>93</sup>. The fertilized yield (YF) is the crop yield under fertilization conditions. The average YS of rice increased from 5.76 t ha<sup>-1</sup> in 2009 to 5.82 t ha<sup>-1</sup> in 2019, and the average YF of rice increased from 8.33 t ha<sup>-1</sup> in 2009 to 8.35 t ha<sup>-1</sup> in 2019; the average YS of maize increased from 4.07 t ha<sup>-1</sup> in 2009 to 4.36 t ha<sup>-1</sup> in 2019, and the average YF of maize increased from 7.04 t ha<sup>-1</sup> in 2009 to 7.17 t ha<sup>-1</sup> in 2019; the average YS of

**Table 1 | Evaluation indices for the prediction accuracy of the RF models**

Model	Crop	Number of training samples	Number of validation samples	R <sup>2</sup>	ME (t ha <sup>-1</sup> )	MAE (t ha <sup>-1</sup> )	RMSE (t ha <sup>-1</sup> )	SMAPE (%)
YS RF	Rice	1072	110	0.89	-0.19	0.79	1.09	14.52
	Maize	460	52	0.93	-0.05	0.90	1.21	24.46
	Wheat	570	63	0.93	0.01	0.56	0.80	21.48
YF RF	Rice	1072	110	0.91	-0.16	0.80	1.04	10.02
	Maize	460	52	0.93	-0.05	0.84	1.14	12.48
	Wheat	570	63	0.93	-0.01	0.67	0.86	15.24

Note: ME, MAE, RMSE, and SMAPE are the mean error, the mean absolute error, the root mean square error, the mean relative error, and the symmetric mean absolute percentage error, respectively.

**Table 2 | RF model prediction results for the crop yield from 2009 to 2019 in Southwest (SW) China**

Crop	Variable	Year	Min. (t ha <sup>-1</sup> )	Median (t ha <sup>-1</sup> )	Max. (t ha <sup>-1</sup> )	Mean (t ha <sup>-1</sup> )	Sum (10 <sup>6</sup> t ha <sup>-1</sup> )	Standard deviation	Coefficient of variation	
Rice	YS	2009	2.89	5.81	7.77	5.76	9.87	0.58	10.01	
		2019	3.49	5.82	7.44	5.82	9.97	0.48	8.19	
	YF	2009	6.24	8.34	9.79	8.33	14.20	0.34	4.04	
		2019	6.31	8.36	9.81	8.35	14.21	0.38	4.53	
	FIY	2009	0.63	2.55	4.64	2.57	4.41	0.52	20.25	
		2019	0.66	2.47	4.21	2.47	4.24	0.52	20.97	
	FCR (%)	2009	8.03	30.38	57.44	30.91	–	0.06	0.20	
		2019	8.73	29.79	49.35	29.78	–	0.06	0.20	
	Maize	YS	2009	1.68	4.07	6.12	4.07	6.33	0.49	12.01
			2019	2.76	4.34	5.89	4.36	6.77	0.39	8.87
YF		2009	5.03	6.93	9.71	7.04	10.94	0.48	6.80	
		2019	5.50	7.06	9.39	7.17	11.16	0.47	6.62	
FIY		2009	0.79	2.94	5.00	2.97	4.62	0.56	19.03	
		2019	1.15	2.77	5.29	2.79	4.33	0.48	17.16	
FCR (%)		2009	12.24	41.98	67.76	42.07	–	0.07	0.16	
		2019	17.95	39.12	62.97	38.96	–	0.05	0.14	
Wheat		YS	2009	1.23	2.80	4.71	2.83	1.65	0.53	18.82
			2019	1.45	2.79	4.61	2.90	1.69	0.52	18.01
	YF	2009	2.93	5.10	7.31	5.20	3.04	0.59	11.34	
		2019	3.14	5.30	7.09	5.34	3.12	0.56	10.47	
	FIY	2009	0.74	2.38	4.08	2.37	1.39	0.39	16.42	
		2019	1.05	2.46	3.65	2.44	1.43	0.33	13.50	
	FCR (%)	2009	20.57	45.66	71.67	45.72	–	0.07	0.15	
		2019	26.43	45.99	63.93	45.93	–	0.06	0.13	

Note: YS, YF, FIY, and FCR denote the soil-based yield, the fertilized yield, the fertilizer increased yield, and the fertilizer contribution ratio, respectively.

wheat increased from 2.83 t ha<sup>-1</sup> in 2009 to 2.90 t ha<sup>-1</sup> in 2019, and the average YF of wheat increased from 5.20 t ha<sup>-1</sup> in 2009 to 5.34 t ha<sup>-1</sup> in 2019. As fertilizer rates decreased over the 10-year period, the improvement in soil nutrients in farmland was probably the main reason for the increase in the crop yield, indicating that China’s policies on farmland protection and systematic fertilization were effective. Compared with YS, fertilization significantly increased the crop yield, increasing the YF of rice increasing by 43.6–44.7%, the YF of maize increasing by 64.7–73.0% and the YF of wheat increasing by 83.9–84.4%. More importantly, fertilization effectively increased the stability of the crop yield<sup>94</sup>; notably, the coefficient of variation (CV) of the rice YS ranged from 8.2 to 10.0%, and that of the rice YF was reduced to 4.0–4.5%; the CV of the maize YS ranged from 8.9 to 12.0%, and that of the maize YF was reduced to 6.6–6.8%; and the CV of the wheat YS ranged from 18.0 to 18.8%, while that of the what YF was reduced to 10.5–11.3%. The spatial distributions of the yields of these three crops in 2009 and 2019 were similar. The crop yields were highest in the western plains due to the flat topography and fertile soils; the crop yields were slightly lower in the southern part of the Yangtze River coast and eastern parallel valleys than in the plains due to the low elevation and favorable light and heat conditions; the crop yields were relatively low in the central hilly areas due to soil nutrient and rainfall limitations; and the mountainous areas around the basin exhibited the lowest crop yields due to their high elevation and complex terrain. In addition, the relatively high fertilizer rates for maize cultivation in East China and North China resulted in relatively high maize YF values in these regions.

Although fertilization is a key factor in increasing crop yields, we observed spatial heterogeneity and a decreasing trend in the contribution of fertilization to crop yields in the study area (Fig. 3). The fertilizer increased yield (FIY) was used to express the increase in the crop yield due to fertilizer

application by subtracting the YS from the YF, and the fertilizer contribution ratio (FCR) was used to measure the contribution of fertilizer to crop yield. For rice, the average FIY value decreased from 2.57 t ha<sup>-1</sup> in 2009 to 2.47 t ha<sup>-1</sup> in 2019, and the average FCR decreased from 30.9% in 2009 to 29.8% in 2019; for maize, the average FIY decreased from 2.97 t ha<sup>-1</sup> in 2009 to 2.79 t ha<sup>-1</sup> in 2019, and the average FCR decreased from 42.1 to 38.9% in 2019; for wheat, the average FIY and FCR essentially remained unchanged. The FIY and FCR of rice and maize generally exhibited the opposite trend to the spatial distribution of crop yields, with the highest values occurring in the central and northern hills and the lowest values occurring in the western plains and along the Minjiang and Yangtze rivers. In contrast, the FIY and FCR of wheat typically followed the crop yield distribution, with higher values in the northern hills and western plains than in the central hills. Therefore, it is necessary to optimize the quantity and distribution of fertilizer inputs to increase nutrient sustainability in Southwest China.

### Widespread crop nutrient imbalances

The nutrient balance assessment results (Figs. 4–6, Table 3 and Supplementary Figs. 2–4) revealed that nutrient imbalance occurred widespread among the three crops in the study area, with an overall excess of nitrogen and deficiencies in phosphorus and potassium. Rice exhibited an excess of nitrogen in most regions, with an average nutrient balance ratio of nitrogen (NBRN) higher than 0.6. The degree of excess nitrogen was higher in the western plains and along the Minjiang and Yangtze rivers, with the actual fertilizer rate in some regions even reaching approximately 10 times the theoretical fertilizer rate. The rice nutrient balance ratio of phosphorus (NBRP) and the nutrient balance ratio of potassium (NBRK) ranged from –0.1 to –0.2, but there was a polarization trend in the spatial distribution. Notably, rice phosphorus and potassium excess areas were distributed in the

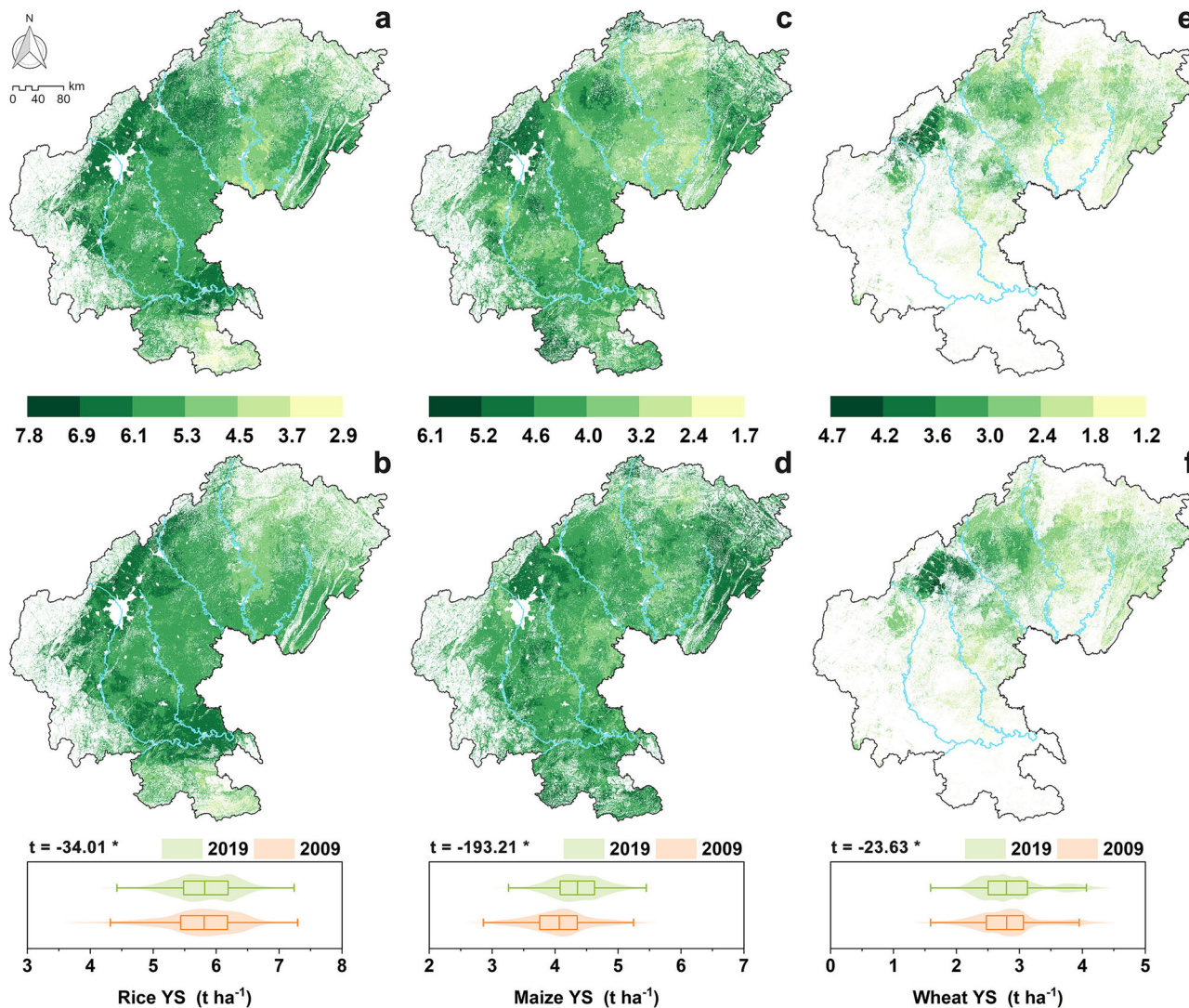


**Fig. 1 | Spatial distributions of the crop soil-based yield (YS) in SW China from 2009 to 2019.** The maps show the spatial distributions of the YS of rice in 2009 (a) and 2019 (b), the spatial distributions of the YS of maize in 2009 (c) and 2019 (d), and the spatial distributions of the YS of wheat in 2009 (e) and 2019 (f). The color bands denote various yield classes ( $t\ ha^{-1}$ ). The box of the violin plot indicates the

interquartile range with the median value shown as a bold line, the whiskers of the violin plot denote the 1.5 interquartile range, and the outer border of the violin plot denotes the data distribution. The symbol  $t$  denotes the value obtained from the  $t$ -test, with the asterisk (\*) indicating that the mean difference between 2009 and 2019 is statistically significant at the 0.05 confidence level.

western plains and along the Minjiang and Yangtze rivers, but there were large phosphorus and potassium deficiency areas in the northeastern and central parts of China. Moreover, the polarization trend in the rice phosphorus and potassium balance increased from 2009 to 2019. For maize, there was a slight excess of nitrogen, with NBRN values ranging from 0.13 to 0.18. Moreover, there was a greater risk of nitrogen excess due to higher nitrogen fertilizer rates for maize in the eastern–central hills and western mountains. The maize NBRP and NBRK values ranged from  $-0.38$  to  $-0.48$ , with significant deficiencies in phosphorus and potassium nutrient inputs, except for a few areas in the west and south. For wheat, nitrogen was generally balanced, with an NBRN value of approximately  $-0.1$ , but there was a risk of increasing nitrogen deficiencies in the northeastern region. Phosphorus and potassium deficiencies were most severe for wheat, with NBRP and NBRK values ranging from  $-0.44$  to  $-0.62$ , and nutrient deficiencies were generally greater in the northern regions.

**Reducing nitrogen fertilizer rates and optimizing nutrient structures can enhance agricultural sustainability**

Due to significant spatial variability in crop nutrient balance ratio (NBR), fertilizer rates should be reduced in areas where  $NBR > 0$  and increased in

areas where  $NBR < 0$ . Therefore, for computational convenience and expression, we adopted the adjustment gradient (%) of fertilizer rates as the optimization variable. The optimal adjustment gradients for nitrogen, phosphorus, and potassium fertilizer for different crops were determined through multiobjective optimization. Taking the optimization of nitrogen fertilizer rates as an example, the greater the adjustment gradient, the closer the fertilizer rate approaches the theoretical fertilizer rate (100% adjustment gradient corresponds to TFRN). Conversely, the smaller the adjustment gradient, the closer the fertilizer rate approaches the fertilizer rate by the farmer’s survey (0% adjustment gradient corresponds to FRN). On the basis of the crop fertilizer rate in 2019 and the theoretical fertilizer rate, regression models of the adjustment gradients of nitrogen fertilizer rates ( $x_1$ ), phosphorus fertilizer rates ( $x_2$ ), and potassium fertilizer rates ( $x_3$ ) with the corresponding total crop yield (OYN, OYP, and OYK) and total fertilizer rate (OFRN, OFRP, and OFRK) were developed (Supplementary Tables 1–9 and Supplementary Figs. 5–22). Table 4 and Fig. 7 show that the regression results for the total nitrogen response yield (OYN), the total phosphorus response yield (OYP), and the total potassium response yield (OYK) could be captured by cubic polynomial regression models with  $R^2$  values ranging from 0.78 to 0.99, whereas

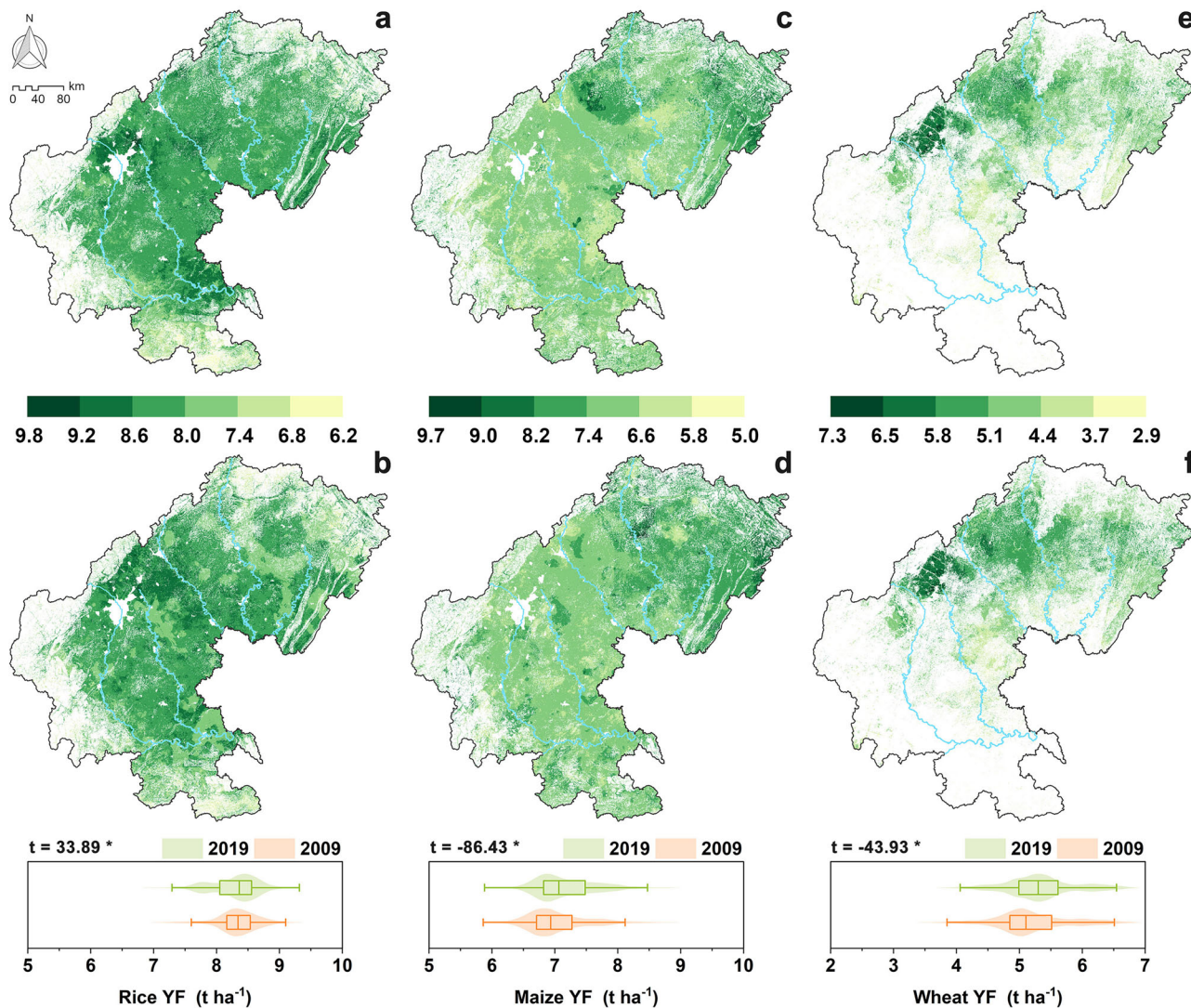


**Fig. 2 | Spatial distributions of the crop fertilized yield (YF) from 2009 to 2019 in SW China.** The maps show the spatial distributions of the YF of rice in 2009 (a) and 2019 (b), the spatial distributions of the YF of maize in 2009 (c) and 2019 (d), and the spatial distributions of the YF of wheat in 2009 (e) and 2019 (f). The color bands denote different yield classes ( $t\ ha^{-1}$ ). The box of the violin plot denotes the

interquartile range with the median value shown as a bold line, the whiskers of the violin plot denote the 1.5 interquartile range, and the outer border of the violin plot indicates the data distribution. The symbol  $t$  denotes the value obtained from the  $t$ -test, with the asterisk (\*) indicating that the mean difference between 2009 and 2019 is statistically significant at the 0.05 confidence level.

those for the total nitrogen fertilizer rate (OFRN), the total phosphorus fertilizer rate (OFRP), and the total potassium fertilizer rate (OFRK) could be represented by primary linear models with  $R^2$  values of 1.00. The above regression models were used as the objective function of the NSGA-II to calculate Pareto solution sets for the fertilizer rate adjustment gradients of rice, maize, and wheat in MATLAB software. These Pareto solution sets contain several preferable solutions (Supplementary Tables 10–12), requiring further identification of the optimal solution with the lowest fertilizer rate and relatively high crop yield. Given the widespread nitrogen excess in the study area, we initially selected 5–6 solutions with the lowest total nitrogen fertilizer rate (OFRN). We then screened these further to identify 2–3 solutions with the lowest total phosphorus (OFRP) or potassium (OFRK) fertilizer rates. The optimal solution was finally identified as the one with the highest overall crop response yield (OYN, OYP, and OYK) among these 2–3 solutions. Figure 7 shows the optimal adjustment gradients for rice nitrogen, phosphorus, and potassium fertilizer rates at 93%, 24%, and 9%, respectively; for maize nitrogen, phosphorus, and potassium fertilizer rates at 83%, 22%, and 9%, respectively; and for wheat nitrogen, phosphorus, and potassium fertilizer rates at 1%, 1%, and 8%, respectively.

According to the optimal adjustment gradient, grid data of the optimal fertilizer rates for the three crops were generated in ArcGIS, and the established RF model was subsequently employed to predict crop yields. Table 5 and Fig. 7 show that the total crop yield in the study area increased by  $13.4 \times 10^4\ t$  after fertilizer rate optimization compared with that in 2019, of which the total rice yield increased by  $8.6 \times 10^4\ t$ , the total maize yield increased by  $4.8 \times 10^4\ t$ , and the wheat yield remained constant. Moreover, the total fertilizer rate in the study area decreased by  $7.9 \times 10^4\ t$  (7.2%) compared with that in 2019, of which the nitrogen fertilizer rate decreased by  $11.3 \times 10^4\ t$  (17.8%), the phosphorus fertilizer rate increased by  $2.4 \times 10^4\ t$  (9.9% increase), and the potassium fertilizer rate increased by  $1.0 \times 10^4\ t$  (5.0%). Among the crops, the fertilizer rates decreased by  $6.8 \times 10^4\ t$  for rice, by  $1.3 \times 10^4\ t$  for maize, and increased slightly ( $0.3 \times 10^4\ t$ ) for wheat. In general, the nitrogen fertilizer rate significantly decreased in the study area, while the nutrient structure was optimized, and the ratio of nitrogen, phosphorus, and potassium fertilizer rates was optimized from 1:0.38:0.33 in 2019 to 1:0.51:0.42, which reached the appropriate nutrient input level for Chinese farmland<sup>95,96</sup>. Optimization mapping of farmland nutrients can accurately reveal the magnitude and distribution of fertilizer rate adjustments (Fig. 8) via the analysis of the spatial changes in crop fertilizer rates

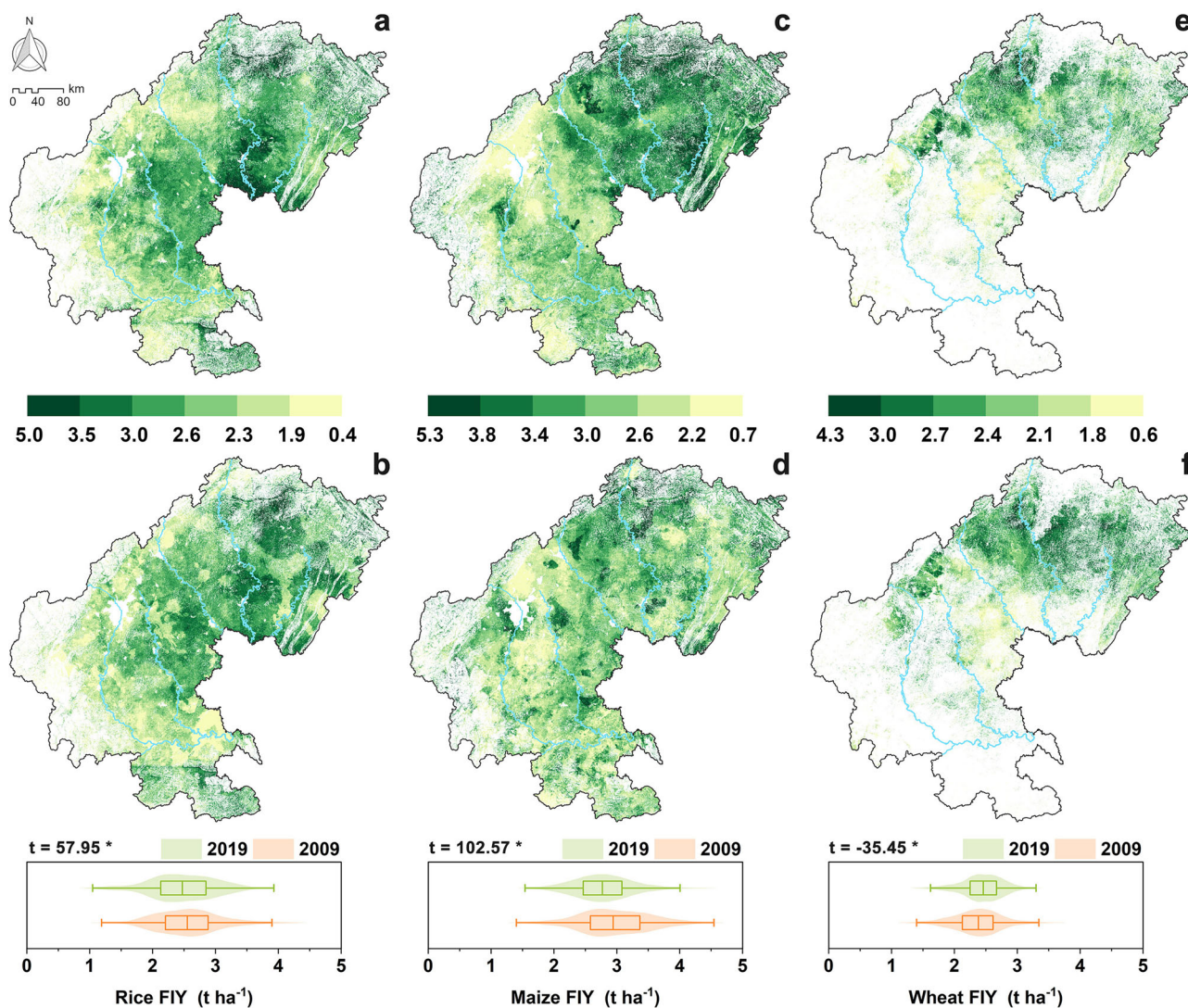


**Fig. 3 | Spatial distributions of the crop fertilizer increased yield (FIY) from 2009 to 2019 in SW China.** The maps show the spatial distributions of the FIY of rice in 2009 (a) and 2019 (b), the spatial distributions of the FIY of maize in 2009 (c) and 2019 (d), and the spatial distributions of the FIY of wheat in 2009 (e) and 2019 (f). The color bands denote various yield classes (t ha<sup>-1</sup>). The box of the violin plot

denotes the interquartile range with the median value shown as a bold line, the whiskers of the violin plot indicate the 1.5 interquartile range, and the outer border of the violin plot denotes the data distribution. The symbol t denotes the value obtained from the t-test, with the asterisk (\*) indicating that the mean difference between 2009 and 2019 is statistically significant at the 0.05 confidence level.

before and after optimization. Obviously, there was spatial heterogeneity in the optimization of fertilizer rates for the three crops. For rice, the nitrogen fertilizer rate must be reduced in most areas, especially in the western plains, along the Minjiang and Fujiang Rivers, and in the lower reaches of the Tuojiang River; the phosphorus and potassium fertilizer rates must be reduced in the western plains and along the Minjiang River but must be increased in the central and northern hills. For maize, the nitrogen fertilizer rate must be reduced in hilly areas on both sides of the Fujiang and Jialingjiang Rivers, but must be moderately increased in the western plains and southern hills; the phosphorus and potassium fertilizer rates must be increased in most areas except along the Minjiang River and in southern mountainous areas. For wheat, the fertilizer rates must be moderately reduced in the central hills and moderately increased in the northern hills and mountains.

### Discussion

The precision management of nutrient resources at the national and regional scales is a key issue for ensuring sustainable agriculture<sup>21</sup>. Over the years, fertilizer field experiments have revealed the quantitative relationship between farmland nutrients and crop yields at the microscale, but due to the

lack of methods for spatially associating and scaling up field experimental data, there is uncertainty in the spatially optimal allocation and management of farmland nutrient resources<sup>91</sup>. On the basis of the widely employed 3414 fertilizer field experimental method in China, an RF prediction model for the crop yield was established under different nutrient conditions, which bridges the gaps in macroscale application of single-point fertilizer field experiments. In an empirical study in Southwest China, we reported that the contribution of fertilizer application to the crop yield decreases with increasing basal soil fertility, whereas the FCR varies across regions (plains < hills < mountains) and crops (rice < maize < wheat), which is consistent with the findings of relevant studies<sup>97–99</sup>. Importantly, our research approach is more advantageous for spatially simulating crop yield responses to nutrient regulation. The general variable importance trend of the RF model was as follows: location factors > meteorological factors > nutrient factors > topographic factors (Supplementary Tables 13–18). Latitude and longitude exhibited the greatest importance, indicating a significant spatial correlation in the crop yield, which further supports the need for spatial optimization of nutrient resources. On one hand, the study area is situated in the transitional zone between the Qinghai–Tibet Plateau and the middle–lower Yangtze River Plain, where location factors significantly

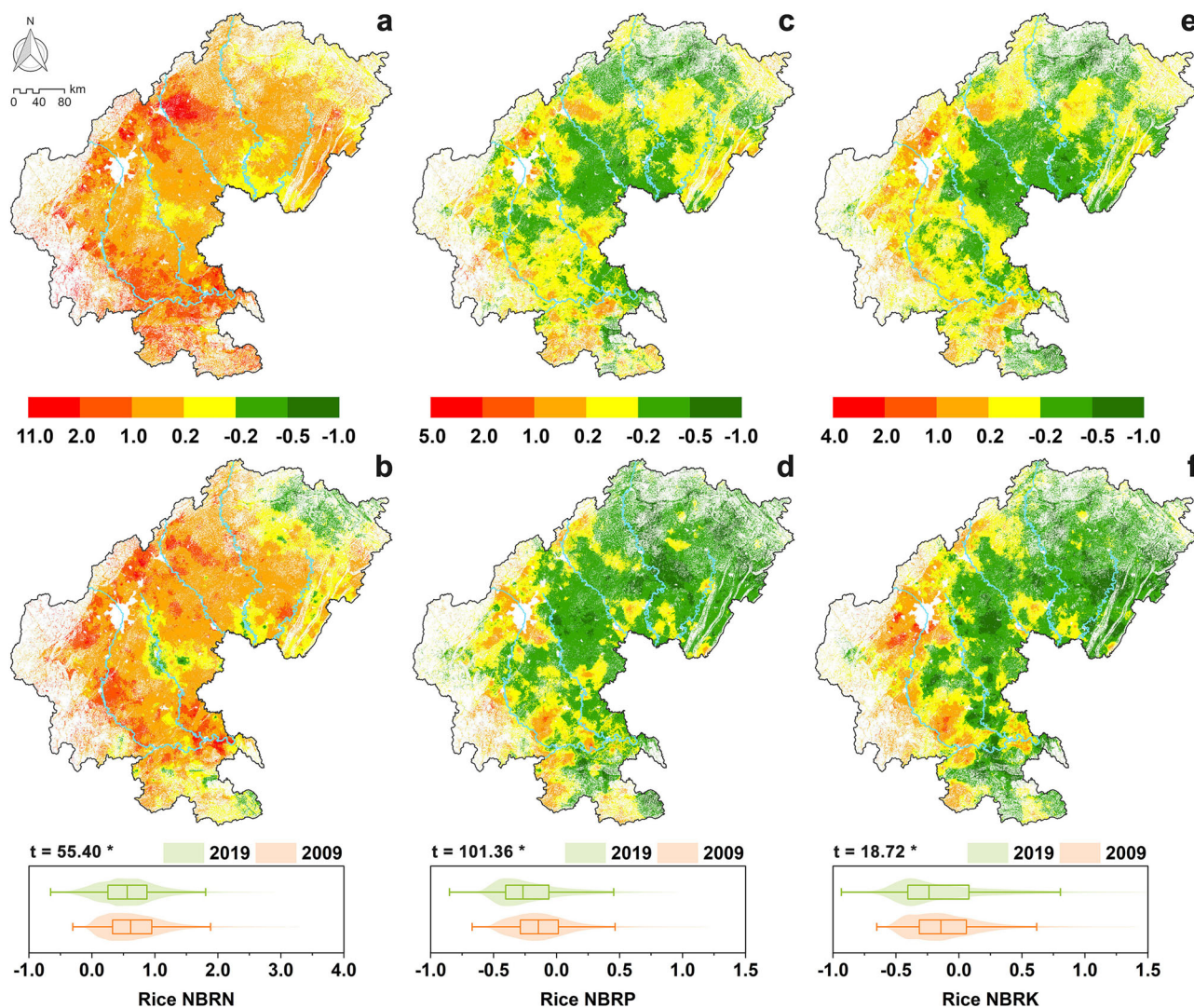


**Fig. 4 | Spatial distributions of the rice nutrient balance ratio from 2009 to 2019 in SW China.** The maps show the spatial distributions of the rice nitrogen nutrient balance ratio (NBRN) in 2009 (a) and 2019 (b), the spatial distributions of the rice phosphorus nutrient balance ratio (NBRP) in 2009 (c) and 2019 (d), and the spatial distributions of the rice potassium nutrient balance ratio (NBRK) in 2009 (e) and 2019 (f). Nutrient balance ratios greater than zero represent excessive fertilizer inputs, ratios equal to zero represent balanced fertilizer inputs, and ratios less than

zero represent insufficient fertilizer inputs. The color bands denote various nutrient balance ratio classes. The box of the violin plot denotes the interquartile range with the median value shown as a bold line, the whiskers of the violin plot indicate the 1.5 interquartile range, and the outer border of the violin plot denotes the data distribution. The symbol *t* denotes the value obtained from the *t*-test, with the asterisk (\*) indicating that the mean difference between 2009 and 2019 is statistically significant at the 0.05 confidence level.

influence the distribution of light and heat resources, thereby affecting crop yield potential<sup>100,101</sup>. On the other hand, relevant studies indicate that crop yield prediction exhibits scale dependency<sup>24</sup>. Variables such as longitude and latitude may be more suitable for large-scale and mesoscale yield prediction models, while such variables may not be necessary in small-scale regions with low spatial autocorrelation. Precipitation and temperature are also important for the crop yield; in particular, precipitation is the most important factor for wheat, but the effect of temperature is significantly lower for maize than for the other crops, which may be due to the more favorable environmental adaptability of maize<sup>102</sup>. The importance of nutrient factors exhibited the order of phosphorus>nitrogen>potassium, and all three crops demonstrated phosphorus sensitivity<sup>103</sup>, indicating that maintaining a phosphorus balance is important for maintaining crop yield stability in the study area. The importance of the vegetation index was moderate for all the RF models, indicating that vegetation information can effectively reflect crop growth trends. Owing to the overall low altitude of the study area, the effect of altitude on the crop yield was limited, while the slope and pH were the least important factors. In addition, there was no significant

difference in the absolute errors of the YS and YF predictions, indicating that the prediction errors may be caused by uncertain factors of crop growth, such as crop varieties, extreme weather, and pests<sup>104-106</sup>. Therefore, yield prediction models should further integrate crop characteristics and adverse environmental factors to increase their accuracy.

In previous macroscale farmland nutrient balance studies, the apparent balance method has been applied, which can hardly reveal the nutrient balance of different crops<sup>54,107</sup>. Moreover, microscale crop nutrient balance assessments are limited to a few field experimental sites<sup>61</sup>, which neglects the spatial application of experimental data. To bridge this research gap, a nutrient balance assessment framework was proposed on the basis of the crop fertilization response. On the one hand, YS and YF values have been obtained under the same environmental conditions in fertilizer field experiments. Thus, the FIY excludes the complex effects of environmental factors other than fertilization, such as nutrients contained in the soil, derived from the atmosphere, and brought in by water, which increases the accuracy and reliability of nutrient demand measurements. On the other hand, this approach facilitates spatial identification and accurate mapping of

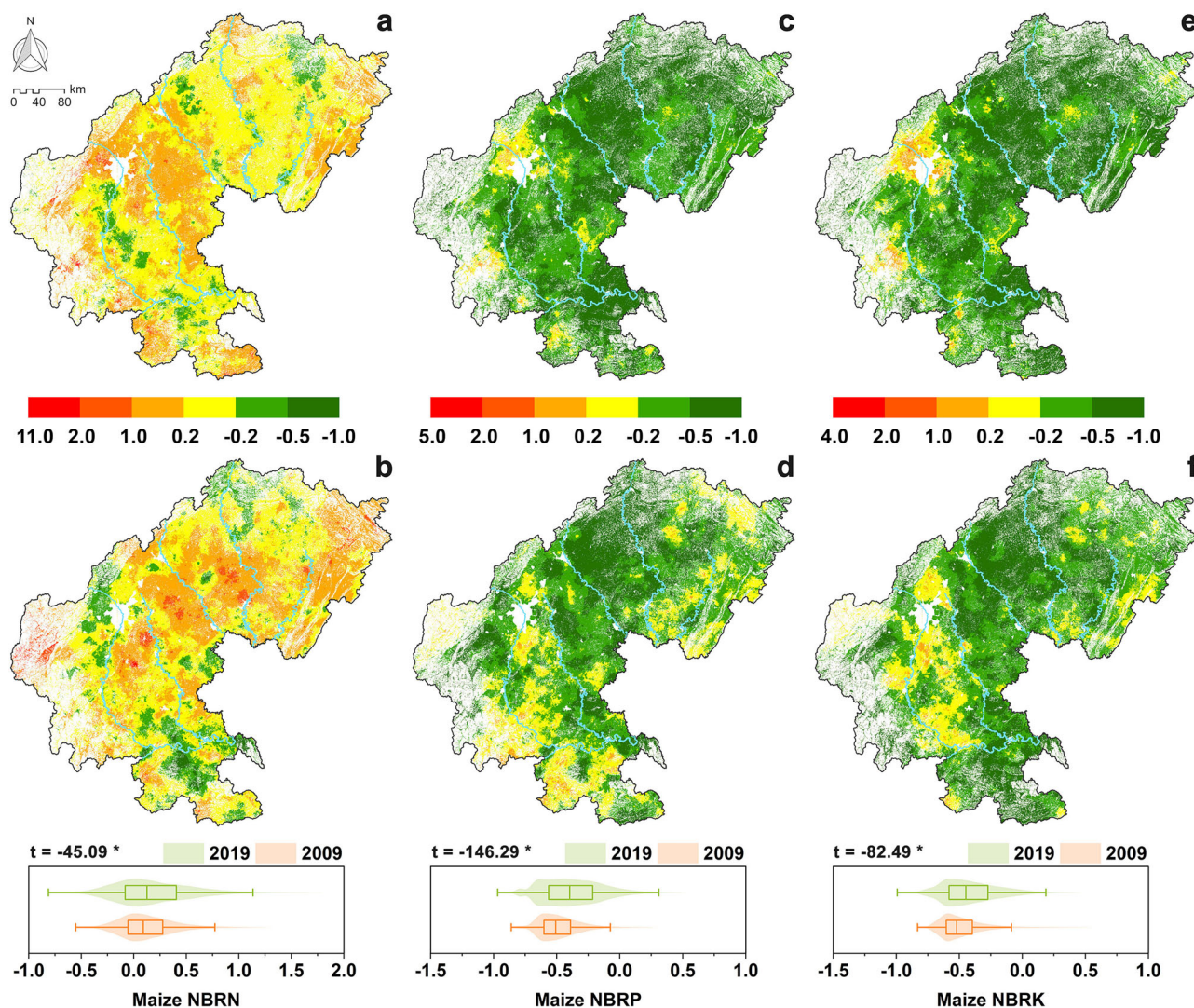


**Fig. 5 | Spatial distributions of the maize nutrient balance ratio from 2009 to 2019 in SW China.** The maps show the spatial distributions of the maize nitrogen nutrient balance ratio (NBRN) in 2009 (a) and 2019 (b), the spatial distributions of the maize phosphorus nutrient balance ratio (NBRP) in 2009 (c) and 2019 (d), and the spatial distributions of the maize potassium nutrient balance ratio (NBRK) in 2009 (e) and 2019 (f). Nutrient balance ratios greater than zero represent excessive fertilizer inputs, ratios equal to zero represent balanced fertilizer inputs, and ratios

less than zero represent insufficient fertilizer inputs. The color bands represent various nutrient balance ratio classes. The box of the violin plot indicates the interquartile range with the median value shown as a bold line, the whiskers of the violin plot denote the 1.5 interquartile range, and the outer border of the violin plot indicates the data distribution. The symbol *t* denotes the value obtained from the *t*-test, with the asterisk (\*) indicating that the mean difference between 2009 and 2019 is statistically significant at the 0.05 confidence level.

the crop nutrient balance, which provides a basis for the next step of optimal regulation of fertilizer inputs. Empirical studies have shown regional and crop differences in nutrient balances in the study area, highlighting the importance of different nutrient management strategies. First, it was confirmed that nitrogen reduction management strategies are particularly important for Southwest China, and the keys to nitrogen regulation are rice and maize in the western plains and along major rivers<sup>54,108,109</sup>. Second, there was widespread phosphorus deficiency in the central and northeastern parts of the study area, especially for maize and wheat, with NBRP values ranging from -0.4 to -0.5, which differs from previous findings of phosphorus excess in Chinese farmlands<sup>10</sup>. On the one hand, the phosphorus fertilizer rate for cash crops is much higher than that for grain crops<sup>55</sup>, so the apparent balance method can reflect only the general trend in farmland phosphorus excess; on the other hand, although the soil phosphorus content increased slightly in the study area, it remained low (soil available phosphorus < 15 mg/kg) in most areas<sup>11</sup>. This phenomenon, coupled with a significant decrease in the phosphorus fertilizer rate per unit area (18 and 13%) for rice and wheat since 2009, has resulted in an increased risk of

phosphorus deficiency for half of the crops. Third, the results of this study confirm the consensus that potassium is widely deficient in Chinese farmlands<sup>112,113</sup>. Although the soil available potassium content has increased in Southwest China over the past decade, the potassium fertilizer rates per unit area for rice and maize have decreased (24% and 7%, respectively), resulting in insufficient potassium inputs<sup>109</sup>. Unexpectedly, the potassium balance of rice showed a polarized trend, which may be related to the fact that farmers in the economically developed regions of the plains and Minjiang River more closely accounted for potassium fertilizer inputs<sup>114</sup>. In addition, owing to the limited number of fertilizer utilization efficiency field experiments, the accuracy of spatial variation simulations for fertilizer utilization efficiency is insufficient. Therefore, the average fertilizer utilization efficiency of Sichuan Basin was used in this study, but the fertilizer utilization efficiency varies by 1–2% across different regions (plains<hills<mountains)<sup>108</sup>, which may cause the theoretical fertilizer rate for crops to be slightly lower than the actual requirements in the plains and slightly higher in the mountains. Therefore, it is necessary to increase the accuracy of determining the fertilizer utilization efficiency in further studies.

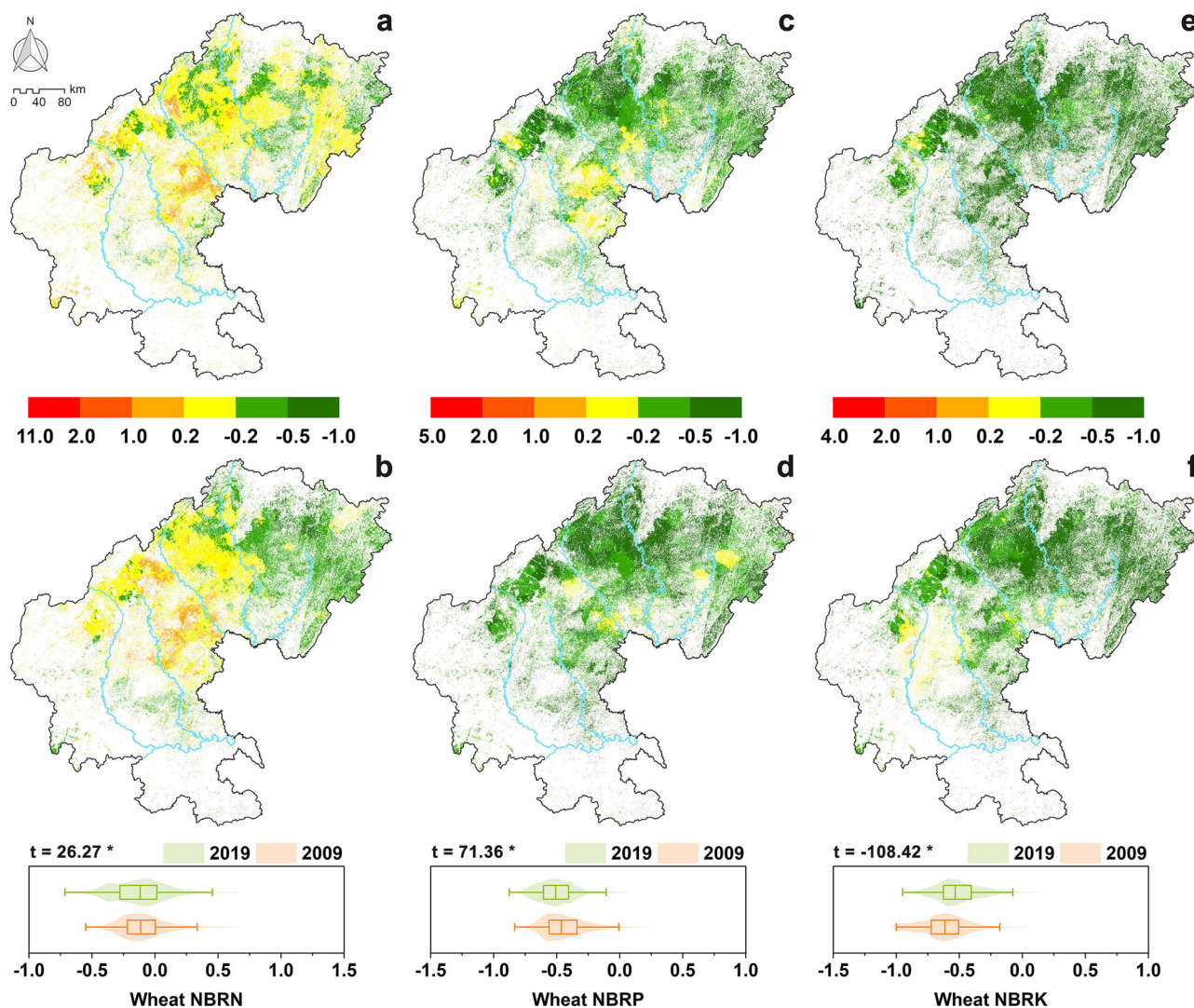


**Fig. 6 | Spatial distributions of the wheat nutrient balance ratio from 2009 to 2019 in SW China.** The maps show the spatial distributions of the wheat nitrogen nutrient balance ratio (NBRN) in 2009 (a) and 2019 (b), the spatial distributions of the wheat phosphorus nutrient balance ratio (NBRP) in 2009 (c) and 2019 (d), and the spatial distributions of the wheat potassium nutrient balance ratio (NBRK) in 2009 (e) and 2019 (f). Nutrient balance ratios greater than zero represent excessive fertilizer inputs, ratios equal to zero represent balanced fertilizer inputs, and ratios

less than zero represent insufficient fertilizer inputs. The color bands represent different nutrient balance ratio classes. The box of the violin plot indicates the interquartile range with the median value as the bold line, the whiskers of the violin plot denote the 1.5 interquartile range, and the outer border of the violin plot indicates the data distribution. The symbol *t* denotes the value obtained from the *t*-test, with the asterisk (\*) indicating that the mean difference between 2009 and 2019 is statistically significant at the 0.05 confidence level.

Finding the optimal balance between food security and ecological security is a relevant and difficult issue in the sustainable management of farmland nutrients<sup>75</sup>. In this study, we adopted a multiobjective NSGA optimization method, which not only aims to provide the optimal solution of fertilizer adjustment but also aims to facilitate the spatial mapping of the optimal solution. The optimization results revealed that the nitrogen fertilizer reduction potential in Southwest China was 17.8%, which is consistent with the range of values of 10–20% estimated in related studies<sup>115,116</sup>. The nitrogen fertilizer reduction potential of rice reached 32.5%, and the average fertilizer rate can be reduced from 136 kg ha<sup>-1</sup> in 2019 to 92 kg ha<sup>-1</sup>, which is higher than the estimates obtained in related studies<sup>117</sup>. The main reason may be that the organic matter and total nitrogen contents in paddy soils (with averages of 26.7 g kg<sup>-1</sup> and 1.47 g kg<sup>-1</sup>, respectively) in the study area are significantly greater than those in dryland soils (with averages of 19.4 g kg<sup>-1</sup> and 1.14 g kg<sup>-1</sup>, respectively), which results in a lower contribution of fertilizer application to the rice yield than that to the yields of the other crops. The highest nitrogen reduction potential of rice was observed in the western plains, where the average soil organic matter and total nitrogen

contents are greater than 30 and 1.7 g kg<sup>-1</sup>, respectively<sup>118</sup>, while the fertilization rate is greater than 150 kg ha<sup>-1</sup>. The maize nitrogen fertilization rate can be reduced by 11.4%, from 206 kg ha<sup>-1</sup> in 2019 to 183 kg ha<sup>-1</sup>, which conforms with related studies<sup>119</sup>. Although there was an increase in the optimized phosphorus and potassium fertilization rates for the three crops, the fertilization rates are still lower than the recommendations of related studies<sup>119–121</sup>, indicating that the fertilization structure in the study area has been optimized to ensure the stability of crop yields.

The ‘field experiment modeling-crop yield prediction-nutrient balance optimization’ methodological framework established in this study has achieved satisfactory results in optimizing fertilizer rates in southwestern China. However, the application of these findings remains limited. Firstly, crop yield prediction variables require regional adjustments; for example, factors such as soil moisture and drought frequency may need to be considered in the arid regions of northern China<sup>122</sup>. Secondly, this approach may not be suitable for high-input intensive systems where nutrient dynamics differ substantially. Greenhouse cultivation systems, for example, suffer from serious nutrient accumulation and continuous cropping issues,

**Table 3 | Nutrient balance statistics for the crop yield from 2009 to 2019 in SW China**

Crop	Variable	Year	Min.	Median	Max.	Mean	Standard deviation
Rice	NBRN	2009	-0.30	0.61	10.69	0.69	0.49
		2019	-0.66	0.56	9.93	0.60	0.50
	NBRP	2009	-0.67	-0.15	4.42	-0.12	0.25
		2019	-0.85	-0.27	2.92	-0.20	0.28
	NBRK	2009	-0.68	-0.15	3.78	-0.10	0.30
		2019	-0.93	-0.24	3.65	-0.12	0.41
Maize	NBRN	2009	-0.57	0.09	4.35	0.13	0.27
		2019	-0.94	0.12	3.22	0.18	0.38
	NBRP	2009	-0.86	-0.51	1.34	-0.48	0.17
		2019	-0.97	-0.40	1.31	-0.38	0.24
	NBRK	2009	-0.83	-0.52	1.91	-0.47	0.20
		2019	-0.99	-0.45	1.00	-0.42	0.23
Wheat	NBRN	2009	-0.60	-0.11	2.26	-0.09	0.18
		2019	-0.73	-0.11	1.21	-0.12	0.21
	NBRP	2009	-0.83	-0.46	1.58	-0.44	0.17
		2019	-0.88	-0.51	0.30	-0.50	0.15
	NBRK	2009	-1.00	-0.61	0.53	-0.62	0.18
		2019	-0.96	-0.53	0.82	-0.51	0.17

Note: NBRN, NBRP, and NBRK denote the crop nutrient balance ratios of nitrogen, phosphorus, and potassium, respectively.

**Table 4 | Regression model for crop fertilizer rate optimization**

Crop	Dependent variable	Independent variable	Model	R <sup>2</sup>
Rice	OYN	x <sub>1</sub>	0.0475 × x <sub>1</sub> <sup>3</sup> + 0.0602 × x <sub>1</sub> <sup>2</sup> - 0.1603 × x <sub>1</sub> + 14.215	1.00
	OYP	x <sub>2</sub>	0.673 × x <sub>2</sub> <sup>3</sup> - 1.2996 × x <sub>2</sub> <sup>2</sup> + 0.782 × x <sub>2</sub> + 14.209	0.83
	OYK	x <sub>3</sub>	0.0766 × x <sub>3</sub> <sup>3</sup> - 0.1254 × x <sub>3</sub> <sup>2</sup> + 0.0216 × x <sub>3</sub> + 14.213	0.99
	OFRN	x <sub>1</sub>	-8.1756 × x <sub>1</sub> + 23.379	1.00
	OFRP	x <sub>2</sub>	2.6425 × x <sub>2</sub> + 9.0894	1.00
	OFRK	x <sub>3</sub>	1.6711 × x <sub>3</sub> + 8.7415	1.00
Maize	OYN	x <sub>1</sub>	0.7336 × x <sub>1</sub> <sup>3</sup> - 1.5089 × x <sub>1</sub> <sup>2</sup> + 0.9009 × x <sub>1</sub> + 11.131	0.88
	OYP	x <sub>2</sub>	0.4113 × x <sub>2</sub> <sup>3</sup> + 0.0008 × x <sub>2</sub> <sup>2</sup> - 0.0095 × x <sub>2</sub> + 11.14	0.96
	OYK	x <sub>3</sub>	1.5791 × x <sub>3</sub> <sup>3</sup> - 2.7217 × x <sub>3</sub> <sup>2</sup> + 1.1573 × x <sub>3</sub> + 11.139	0.78
	OFRN	x <sub>1</sub>	-4.4209 × x <sub>1</sub> + 32.157	1.00
	OFRP	x <sub>2</sub>	7.8178 × x <sub>2</sub> + 11.834	1.00
	OFRK	x <sub>3</sub>	7.1662 × x <sub>3</sub> + 9.3479	1.00
Wheat	OYN	x <sub>1</sub>	-0.0764 × x <sub>1</sub> <sup>3</sup> + 0.1283 × x <sub>1</sub> <sup>2</sup> - 0.0161 × x <sub>1</sub> + 3.1151	0.82
	OYP	x <sub>2</sub>	-0.1503 × x <sub>2</sub> <sup>3</sup> + 0.1452 × x <sub>2</sub> <sup>2</sup> + 0.0171 × x <sub>2</sub> + 3.1183	0.81
	OYK	x <sub>3</sub>	-0.1392 × x <sub>3</sub> <sup>3</sup> + 0.2377 × x <sub>3</sub> <sup>2</sup> - 0.0826 × x <sub>3</sub> + 3.1231	0.99
	OFRN	x <sub>1</sub>	1.273 × x <sub>1</sub> + 7.8869	1.00
	OFRP	x <sub>2</sub>	3.382 × x <sub>2</sub> + 3.2518	1.00
	OFRK	x <sub>3</sub>	3.1016 × x <sub>3</sub> + 2.8368	1.00

Note: the independent variables x<sub>1</sub>, x<sub>2</sub>, and x<sub>3</sub> denote the adjustment gradients (%) of the nitrogen, phosphorus, and potassium fertilizer rates, respectively; OFRN, OFRP, and OFRK are the total nitrogen fertilizer rate, total phosphorus fertilizer rate, and total potassium fertilizer rate, respectively; OYN, OYP, and OYK denote the total nitrogen response yield, total phosphorus response yield, and total potassium response yield, respectively.

resulting in distinct crop nutrient demand patterns compared to field crops. This makes it difficult to establish models such as fertilizer effect functions and nutrient balance<sup>123</sup>. Thirdly, constrained by computational efficiency, the computational complexity was reduced by fitting a linear model of the gradient adjustment and yield and fertilizer rates without implementing grid-by-grid iterative NSGA optimization, which will be further explored and addressed in our future research. Notably, since 2020, the Chinese

government has launched a new round of fertilizer reduction initiatives<sup>124</sup>, mandating further decreases in fertilizer rates and implementing quota management for nitrogen fertilizers in crops, thereby providing extensive application scenarios for the methodological framework developed in this study. Next, we will utilize the latest soil and field experiment data to conduct research, aiming to provide decision-making references for the precise management of farmland nutrient resources in China.

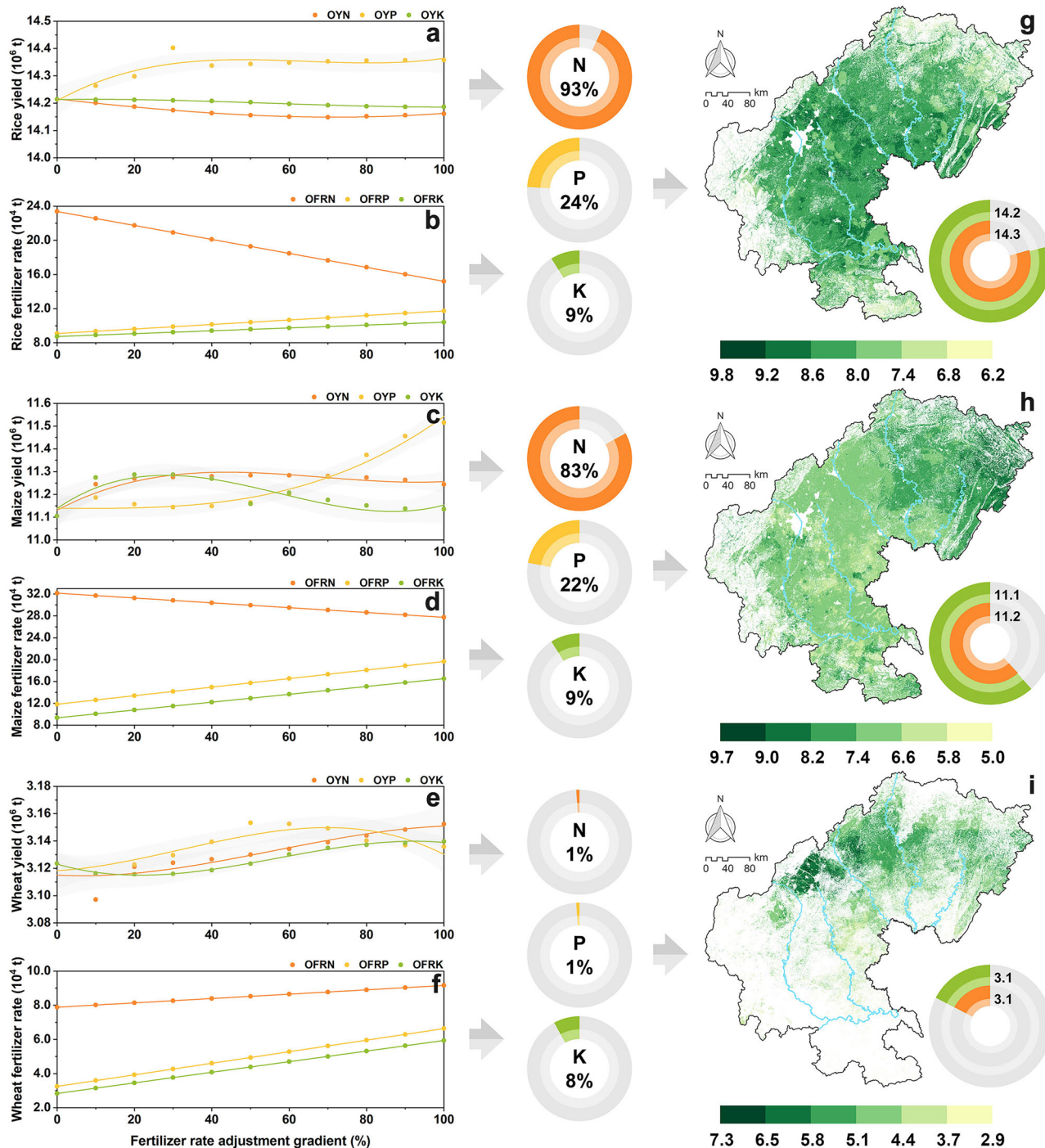


**Fig. 7 | Multiobjective NSGA optimization of the crop fertilizer rate in SW China.** Regression models of the fertilizer rate adjustment gradient with the total nitrogen response yield (OYN), total phosphorus response yield (OYP) and total potassium response yield (OYK): Rice (a), maize (c), and wheat (e). Regression models of the fertilizer rate adjustment gradient with the total nitrogen fertilizer rates (OFRN), total phosphorus fertilizer rates (OFRP), and total potassium fertilizer rates (OFRK): Rice (b), maize (d), and wheat (f). The ring charts in the middle show the optimal

adjustment gradients (%) of the nitrogen, phosphorus and potassium fertilizer rates calculated by the NSGA for the 3 crops. The maps on the right show the yields (t ha<sup>-1</sup>) of rice (g), maize (h), and wheat (i) after fertilizer rate optimization. The ring charts in the map show the total crop yield (10<sup>6</sup> t), with the green color denoting the total YF in 2019 and the orange color denoting the total YF after fertilizer rate optimization.

## Methods

### Study area

The Sichuan Basin, one of China’s four major basins, is located in the southern–central part of the Asian continent (28°–32°N, 102°–108°E) and is surrounded by the Tibetan Plateau, Yunnan–Guizhou Plateau, Wushan Mountains, and Daba Mountains. The total size of the study area is

approximately 18 × 10<sup>4</sup> km<sup>2</sup> (Fig. 9), with plains and hills in the central part (250–750 m altitude) surrounded by mountains (1000–3000 m altitude). The surface of the basin is covered by Mesozoic purple–red sandstone and mudstone, forming the largest purple soil distribution area in China. The climate is warm and humid, and the area belongs to the mid-subtropical humid climate zone, with an average annual temperature of 16–18 °C, an

**Table 5 | Comparison of the crop fertilizer rates and yields before and after optimization in SW China**

Crop	Optimization	OFRN (10 <sup>4</sup> t)	OFRP (10 <sup>4</sup> t)	OFRK (10 <sup>4</sup> t)	FRN (kg ha <sup>-1</sup> )	FRP (kg ha <sup>-1</sup> )	FRK (kg ha <sup>-1</sup> )	Total fertilizer rate (10 <sup>4</sup> t)	Total yield (10 <sup>6</sup> t)
Rice	Before	23.38	9.09	8.74	136.36	53.01	50.98	41.21	14.21
	After	15.78	9.72	8.89	92.02	56.72	51.86	34.39	14.30
Maize	Before	32.16	11.84	9.35	206.77	76.09	60.11	53.35	11.10
	After	28.49	13.55	9.99	183.19	87.15	64.25	52.03	11.15
Wheat	Before	7.89	3.25	2.84	134.77	55.57	48.47	13.98	3.12
	After	7.88	3.29	3.08	134.76	56.14	52.72	14.25	3.12
Total	Before	63.43	24.18	20.93	–	–	–	108.54	28.44
	After	52.14	26.56	21.97	–	–	–	100.67	28.57

Note: FRN, FRP, and FRK denote the actual nitrogen, phosphorus, and potassium fertilizer rates per unit area of crops, respectively.

annual precipitation of 1000–1200 mm, an annual accumulated temperature of 4000–6000 °C, and an annual sunshine duration of only 1000–1400 h; hence, the area receives the least sunshine in China<sup>125</sup>. The number of rivers in the basin exceeds one thousand, with runoff exceeding 250 billion m<sup>3</sup>, and the famous Yangtze River originates in the southern part of the basin. The Chengdu–Chongqing urban agglomeration in the Sichuan Basin is one of the most economically developed regions in China, with a population of more than 75 million people, a gross domestic product (GDP) of more than 5 trillion CNY, and an urbanization rate of 60%. Moreover, grain has been cultivated in the region for more than 3000 years, and the current annual grain yield is above 28 million tons, making it the most important grain-producing area in Southwest China. However, due to long-term irrational fertilization, the consumption of chemical fertilizers in the region exceeds 300 kg ha<sup>-1</sup> (that of N exceeds 140 kg ha<sup>-1</sup>)<sup>126</sup>, leading to serious problems such as greenhouse gas emissions and water pollution by nitrogen and phosphorus<sup>83,84</sup>. The fertilizer inputs in the Sichuan Basin are much higher than the international average<sup>95</sup>, with agricultural nonpoint source pollution already at the moderate risk level<sup>127</sup>. The optimal regulation of nutrient resources in farmlands in the Sichuan Basin is therefore important for ensuring environmental protection and food security in the upper reaches of the Yangtze River in China.

**Data sources and processing**

Spatial distribution data (30 × 30 m) of rice, maize, and wheat for the study area were obtained from the National Ecosystem Science Data Center<sup>128–130</sup>. Soil and fertilizer rate data were collected from the *Soil Testing and Formulated Fertilization Project (STFF)* and the *Cultivated Land Quality Monitoring Project (CLQM)* of Sichuan Province. A total of 20,798 and 17,737 surface soil samples (0–20 cm) from cropland were collected in the study area in 2009 and 2019 (Fig. 10), respectively, and the soil property indicators included organic matter (OM), pH, available phosphorus (AP), and available potassium (AK) (Supplementary Table 19). The nitrogen fertilizer rate (FRN), phosphorus fertilizer rate (FRP), and potassium fertilizer rate (FRK) for rice, maize, and wheat were obtained from a farmer’s fertilization survey, which included 3918 and 3344 samples for rice, 4212 and 3592 samples for maize, and 1591 and 957 samples for wheat in 2009 and 2019, respectively (Table 6 and Supplementary Table 20). The method of fertilization survey refers to the Technical Code for Cultivated Land Quality Monitoring (NY/T 1119). FRN, FRP, and FRK were calculated for each crop cultivation survey site based on the nutrient content, dosage, and frequency of fertilizers. The formula can be expressed as

$$FRN = \sum_{i=1}^n (NCN_i \times Q_i) \tag{1}$$

$$FRP = \sum_{i=1}^n (NCP_i \times Q_i) \tag{2}$$

$$FRK = \sum_{i=1}^n (NCK_i \times Q_i) \tag{3}$$

where FRN, FRP, and FRK refers to the nitrogen fertilizer rate (N), phosphorus fertilizer rate (P<sub>2</sub>O<sub>5</sub>), potassium fertilizer rate (K<sub>2</sub>O) during the growth period of rice (kg ha<sup>-1</sup>); n refers to the frequency of fertilization during the growth period of rice; *NCN<sub>i</sub>*, *NCP<sub>i</sub>*, and *NCK<sub>i</sub>* refers to the N, P<sub>2</sub>O<sub>5</sub>, and K<sub>2</sub>O contents of the *i* times of fertilization (%), respectively; *Q<sub>i</sub>* refers to the actual rate of the *i* times fertilizer (kg ha<sup>-1</sup>).

Geostatistical methods were used to predict the spatial distributions of soil properties and fertilizer rates<sup>131,132</sup>. The Kolmogorov-Smirnov (K-S) method was used in SPSS 24 software for testing the normal distribution of the original data. Finally, we used a logarithmic transformation to make pH, AP, AK, FRN, FRP, and FRK conform to normal distributions to meet the requirements of geostatistical analysis. Geostatistics is based on the theory of regionalized variables and uses semi-variance functions as the main tool to reveal the spatial distribution, variation, and related characteristics of attribute variables. Geostatistical analysis has been widely applied in the study of the spatial distribution of soil and fertilizers. The semi-variance function is the key to geostatistical analysis, reflecting the degree of the spatial autocorrelation of observations at different distances. The model can be expressed as

$$\gamma(h) = \frac{1}{2N(h)} \sum_{i=1}^{N(h)} [Z(x_i) - Z(x_i + h)]^2 \tag{4}$$

where  $\gamma(h)$  refers to the semi-variance function; h refers to the step size; N(h) refers to the logarithm of the observed sample points, and  $Z(x_i)$  and  $Z(x_i + h)$  refer to the measured values of the variable Z(x) at the spatial positions  $x_i$  and  $x_i + h$ , respectively.

The ratio of Nugget to Sill  $C_0/(C_0 + C)$  can indicate the degree of spatial heterogeneity caused by random factors, which is often used as a classification basis for spatial correlation of variables.  $C_0/(C_0 + C)$  less than 25% indicates strong spatial correlation;  $C_0/(C_0 + C)$  is a moderate spatial correlation between 25 and 75%;  $C_0/(C_0 + C)$  greater than 75% indicates weak spatial correlation. We used GS+ software to fit the semi-variance function model of each indicator, and after repeated simulations, we ultimately selected the optimal fitting function to obtain the semi-variance function graph (Supplementary Fig. 23 and Supplementary Fig. 24) and structural parameters (Supplementary Tables 21 and 22). The results showed that each soil and fertilizer index had a good semi-variance structure and spatial correlation. Error analysis revealed that the geostatistical spatial distribution predictions were reliable. ArcGIS was used to map the spatial distribution of each factor (Supplementary Fig. 25–29).

Fertilizer field experimental data were collected from the STFF of the Sichuan Basin, including 2327 experiments (rice: 1182; maize: 512; wheat: 633) from 2009 to 2019 (Fig. 10). These experiments relied on the “3414”

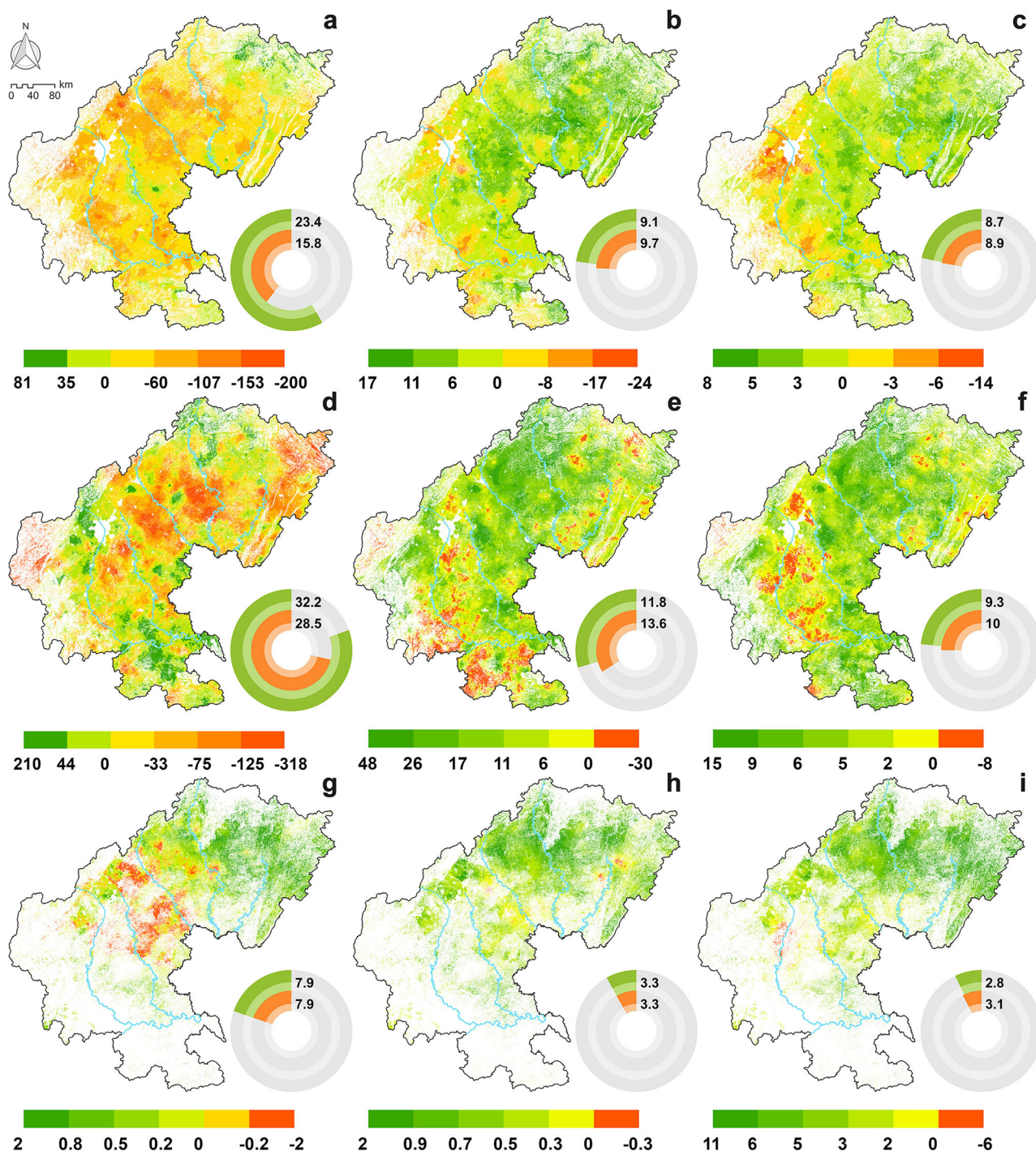


**Fig. 8 | Spatial optimization of farmland nutrients in SW China.** The maps show the spatial distributions of the optimized adjustments of the rice, maize and wheat fertilizer rates (a positive value indicates an increase in the fertilizer rate, whereas a negative value indicates a decrease in the fertilizer rate): **a–c** Changes in the rice nitrogen, phosphorus and potassium fertilizer rates (kg ha<sup>-1</sup>); **d–f** changes in the

maize nitrogen, phosphorus and potassium fertilizer rates (kg ha<sup>-1</sup>); **g–i** changes in the wheat nitrogen, phosphorus and potassium and potassium fertilizer rates (kg ha<sup>-1</sup>). The ring charts show the total fertilizer rate (10<sup>4</sup> t), with the green color indicating the total fertilizer rate in 2019 and the orange color representing the total fertilizer rate after optimization.

design scheme, which was proposed by the Chinese Ministry of Agriculture. The “3414” field experiment is not a long-term experiment and is usually conducted for one or several years at each site. All fertilizer field experiments were conducted by technicians from county agricultural government departments to ensure the reliability of the test results. The “3414” field experiment refers to 3 factors (nitrogen, phosphorus, and potassium), 4 fertilization levels (0, 1, 2, and 3), and 14 treatments<sup>95</sup>. Four fertilization levels were employed: level 0 refers to no fertilization; level 2 refers to the

representative fertilization rate of the experimental area (N, P<sub>2</sub>O<sub>5</sub>, and K<sub>2</sub>O); level 1 = level 2 × 0.5 (this level represents insufficient fertilization); and level 3 = level 2 × 1.5 (this level represents excessive fertilization). The 14 experimental treatments were (1) N<sub>0</sub>P<sub>0</sub>K<sub>0</sub>, (2) N<sub>0</sub>P<sub>2</sub>K<sub>2</sub>, (3) N<sub>1</sub>P<sub>2</sub>K<sub>2</sub>, (4) N<sub>2</sub>P<sub>0</sub>K<sub>2</sub>, (5) N<sub>2</sub>P<sub>1</sub>K<sub>2</sub>, (6) N<sub>2</sub>P<sub>2</sub>K<sub>2</sub>, (7) N<sub>2</sub>P<sub>3</sub>K<sub>2</sub>, (8) N<sub>2</sub>P<sub>2</sub>K<sub>0</sub>, (9) N<sub>2</sub>P<sub>2</sub>K<sub>1</sub>, (10) N<sub>2</sub>P<sub>2</sub>K<sub>3</sub>, (11) N<sub>3</sub>P<sub>2</sub>K<sub>2</sub>, (12) N<sub>1</sub>P<sub>1</sub>K<sub>2</sub>, (13) N<sub>1</sub>P<sub>2</sub>K<sub>1</sub>, and (14) N<sub>2</sub>P<sub>1</sub>K<sub>1</sub> (Supplementary Table 23). The ‘3414’ field experiment is described in Supplementary Note 1.

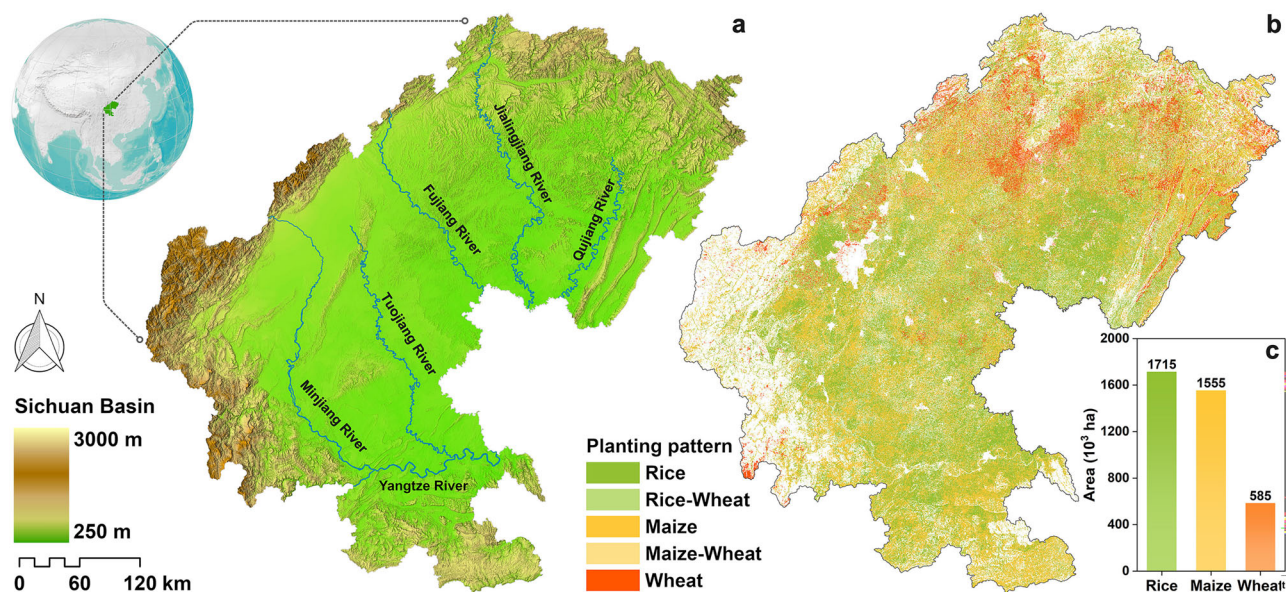


**Fig. 9 | Map of the location, landforms and crop distribution in SW China.** **a** Location and landforms of the study area. The colors denote the altitude (m) of the study area. The blue lines denote the major rivers. **b** Distribution of rice, maize, and wheat planting areas and patterns. **c** Statistical chart of rice, maize, and wheat planting areas ( $10^3$  ha).

The Resource and Environmental Science Data Platform provides spatial datasets of digital elevation models (DEMs), annual mean precipitation (PRE), annual mean temperature (TEM), NDVI values at the crop maturity stage, roads, rivers, and administrative districts<sup>133–136</sup>. These grid data were converted to a uniform spatial resolution ( $30 \times 30$  m) via ArcGIS 10.8 (Supplementary Table 25 and Supplementary Figs. 28 and 29). Socio-economic data were collected from the *Statistical Yearbook of Sichuan Province*<sup>126,137</sup>.

### Crop yield prediction under different nutrient conditions

The RF algorithm is a machine learning algorithm that integrates many classification and regression trees (CARTs) and involves the use of a double random sampling method to avoid overfitting<sup>43</sup>. RF regression analysis first involves constructing  $n$  regression trees by randomly selecting a subset of  $n$  samples from the original sample using the bootstrap method. The remaining samples constitute out-of-bag (OOB) data each time for error estimation and variable importance evaluation. Second, while each tree is generated,  $m$  variables ( $m < M$ ) are randomly selected from the set of  $M$  explanatory variables, and the optimal branches are recursively selected via the mean square deviation as a node splitting criterion. Finally, the average of all the decision tree predictions is adopted as the final result<sup>138</sup>. In this work, RF yield prediction models for rice, maize and wheat were established in ArcGIS software using 2327 fertilizer field experiments (approximately 90% of the data were randomly selected as training samples, and approximately 10% of the data were used as validation samples) (Fig. 10). After several fitting comparison steps, the RF model parameters were set as follows: the number of decision trees is 1000, the minimum leaf size is 5, the number of randomly sampled variables is the square root of the total number of explanatory variables, and the remaining parameters were set to software default values.

Our previous study revealed that the crop nutrient balance can be effectively evaluated by predicting crop yields under different nutrient conditions (nonfertilization and fertilization)<sup>118</sup>. Therefore, we established RF prediction models for the soil-based yield (YS) and fertilized yield (YF) of the three crops. The YS refers to the crop yield in the current year without fertilization, reflecting the inherent soil productivity of farmland, and it can be expressed as the yield of treatment 1 ( $N_0P_0K_0$ ) under the 3414 experimental scheme. The YS prediction model included 11 explanatory variables: longitude ( $X_1$ ), latitude ( $X_2$ ), altitude ( $X_3$ ), slope ( $X_4$ ), soil OM ( $X_5$ ), soil pH ( $X_6$ ), soil AP ( $X_7$ ), soil AK ( $X_8$ ), PRE ( $X_9$ ),

TEM ( $X_{10}$ ), and the NDVI at the crop maturity stage ( $X_{11}$ ). The YF denotes the crop yield under fertilization conditions, which can be expressed as the yield of treatment 6 ( $N_2P_2K_2$ ) under the 3414 experimental scheme. The number of explanatory variables of the YF model was 14, with the addition of three fertilization rate variables: FRN ( $X_{12}$ ), FRP ( $X_{13}$ ), and FRK ( $X_{14}$ ). Supplementary Table 24 shows the statistics of rice YS (treatment 1), YF (treatment 6), and fertilizer rate (level 2) for all “3414” field experimental points in this study. The fertilizer increased yield (FIY) was used to express the increase in the crop yield due to fertilizer application by subtracting the YS from the YF. Since the YS and YF were obtained under the same natural and farm management conditions in the field experiments, the FIY can reliably reveal the independent effect of fertilization on the crop yield by excluding soil nutrient differences<sup>139</sup>. The fertilizer contribution ratio (FCR) was used to measure the contribution of fertilizer to crop yield<sup>140</sup>. The calculation is as follows:

$$YS = G(X_k), X_k = X_1, X_2, \dots, X_{11} \quad (5)$$

$$YF = H(X_k), X_k = X_1, X_2, \dots, X_{14} \quad (6)$$

$$FIY = YF - YS \quad (7)$$

$$FCR = (YF - YS)/YF \times 100\% \quad (8)$$

where YS, YF, FIY and FCR denote the soil-based yield ( $\text{kg ha}^{-1}$ ), the fertilized yield ( $\text{kg ha}^{-1}$ ), the fertilizer increased yield ( $\text{kg ha}^{-1}$ ) and the fertilizer contribution ratio (%), respectively, in each crop planting grid ( $30 \times 30$  m);  $G(X_k)$  and  $H(X_k)$  denote the YS and YF RF prediction models, respectively, established in the field experiments; and  $X_k$  is the value of the explanatory variable  $k$  in each crop planting grid.

To evaluate the simulation accuracy of the RF model, we randomly selected 225 field experiments (rice: 110; maize: 52; wheat: 63) as validation samples to calculate the error between the actual and predicted yields (Fig. 10). The evaluation metrics can be calculated as follows:

$$ME = 1/n \sum_{i=1}^n \{z(x_i) - z'(x_i)\} \quad (9)$$

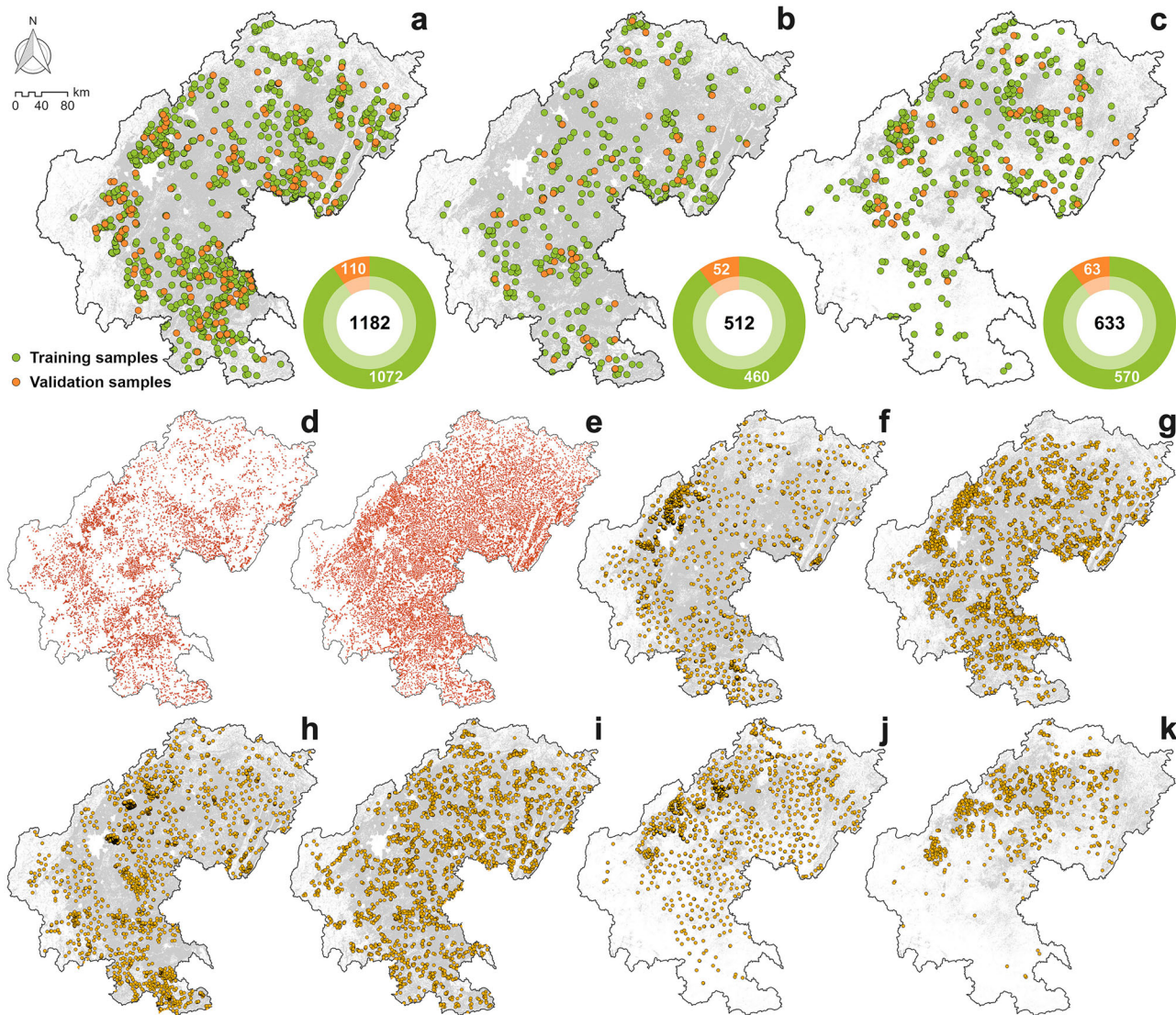


**Fig. 10 | Distribution of fertilizer field experiments, soil samples and fertilization survey samples in SW China.** The gray fills in the map indicate the planting areas of rice, maize, or wheat. The ring chart shows the number of fertilizer field experiments (green denotes the number of training samples, and orange denotes the number of validation samples). **a** Rice fertilizer field experiments. **b** Maize fertilizer field

experiments. **c** Wheat fertilizer field experiments. **d** Soil sample sites in 2009. **e** Soil sample sites in 2019. **f** Rice fertilization survey sites in 2009. **g** Rice fertilization survey sites in 2019. **h** Maize fertilization survey sites in 2009. **i** Maize fertilization survey sites in 2019. **j** Wheat fertilization survey sites in 2009. **k** Wheat fertilization survey sites in 2019.

**Table 6 | Statistics of crop field experiments, soil and fertilizer survey samples in SW China**

Type	Crop	Year	Number of samples
Soil sample	-	2009	20798
		2019	17737
Fertilizer survey sample	Rice	2009	3918
		2019	3344
	Maize	2009	4212
		2019	3592
	Wheat	2009	1591
		2019	957
Fertilizer field experiment	Rice	2009–2019	1182
	Maize	2009–2019	512
	Wheat	2009–2019	633

$$MAE = 1/n \sum_{i=1}^n \{|z(x_i) - z'(x_i)|\} \tag{10}$$

$$RMSE = \sqrt{1/n \sum_{i=1}^n \{z(x_i) - z'(x_i)\}^2} \tag{11}$$

$$SMAPE = 1/n \sum_{i=1}^n \{(2 \times |z(x_i) - z'(x_i)|) / (|z(x_i)| + |z'(x_i)|)\} \times 100\% \tag{12}$$

where ME, MAE, RMSE, and SMAPE are the mean error, the mean absolute error, the root mean square error, the mean relative error, and the symmetric mean absolute percentage error, respectively;  $z'(x_i)$  is the predicted value of sample  $i$ ;  $z(x_i)$  is the actual observed value of sample  $i$ ; and  $n$  is the number of samples. The smaller the MAE, RMSE, and SMAPE values are, the smaller the error and the higher the simulation accuracy.

**Table 7 | The average nutrient uptake per 100 kg of the crop yield and the fertilizer utilization efficiency in the Sichuan Basin, SW China**

Crop	Number of samples	NUTN (kg)	NUTP (kg)	NUTK (kg)	REN (%)	REP (%)	REK (%)
Rice	89	1.41	0.70	1.26	39.34	25.31	51.33
Maize	92	2.16	0.90	1.91	33.72	19.83	50.08
Wheat	33	2.27	0.66	1.75	35.42	14.22	42.12

Note: NUTN, NUTP, and NUTK denote nitrogen, phosphorus, and potassium nutrient uptake values (kg) per 100 kg of the crop yield, respectively; REN, REP, and REK denote the crop nitrogen, phosphorus, and potassium fertilizer utilization efficiency values (%), respectively.

### Crop nutrient balance assessment

The spatial distributions of the nutrient balances for the three crops were evaluated according to our previous research methodology<sup>18</sup>. First, the average nutrient uptake per 100 kg of the crop yield<sup>141</sup> and the fertilizer utilization efficiency<sup>142,143</sup> were calculated for the three crops using 214 fertilizer utilization efficiency field experiments in the Sichuan Basin (Table 7 and Supplementary Fig. 30). Second, on the basis of the nutrient balance method<sup>144</sup>, the theoretical fertilizer rates for the three crops were calculated using the FIY prediction results. Finally, the theoretical fertilizer rate was compared with the actual fertilizer rate to calculate the nutrient balance ratios of nitrogen, phosphorus, and potassium for the three crops<sup>61</sup>. The calculation is as follows:

$$NUTN = [Y_{SE} \times NCN_{SE} + Y_{SL} \times NCN_{SL} \times (1 - SR)] / Y_{SE} \times 100 \quad (13)$$

$$NUTP = [Y_{SE} \times NCP_{SE} + Y_{SL} \times NCP_{SL} \times (1 - SR)] / Y_{SE} \times 100 \quad (14)$$

$$NUTK = [Y_{SE} \times NCK_{SE} + Y_{SL} \times NCK_{SL} \times (1 - SR)] / Y_{SE} \times 100 \quad (15)$$

$$REN = NUTN \times (Y_{NPK} - Y_{PK}) / FerN \times 100 \quad (16)$$

$$REP = NUTP \times (Y_{NPK} - Y_{NK}) / FerP \times 100 \quad (17)$$

$$REK = NUTK \times (Y_{NPK} - Y_{NP}) / FerK \times 100 \quad (18)$$

where *NUTN*, *NUTP* and *NUTK* denote nitrogen, phosphorus and potassium nutrient uptake values (kg) per 100 kg of the crop yield, respectively; *Y<sub>SE</sub>* and *Y<sub>SL</sub>* are the crop seed yield and stem-leaf yield (kg ha<sup>-1</sup>), respectively; *NCN<sub>SE</sub>* and *NCN<sub>SL</sub>* denote the total nitrogen contents (g kg<sup>-1</sup>) in crop seeds and stems-leaves, respectively; *NCP<sub>SE</sub>* and *NCP<sub>SL</sub>* denote the total phosphorus contents (g kg<sup>-1</sup>) in crop seeds and stems-leaves, respectively; and *NCK<sub>SE</sub>* and *NCK<sub>SL</sub>* denote the total potassium contents (g kg<sup>-1</sup>) in crop seeds and stems-leaves, respectively; and *SR* is the rice straw return rate. According to relevant research<sup>145</sup>, the straw return rates for rice, maize, and wheat in the Sichuan Basin are 63.64%, 42.36% and 40.55%, respectively. Moreover, *REN*, *REP* and *REK* denote the crop nitrogen, phosphorus and potassium fertilizer utilization efficiency values (%), respectively; *Y<sub>NPK</sub>* denotes the crop yield under the field experiment treatment using nitrogen, phosphorus and potassium fertilizers; *Y<sub>PK</sub>* is the crop yield under the field experiment treatment using phosphorus and potassium fertilizers; *Y<sub>NK</sub>* denotes the crop yield under the field experiment treatment using nitrogen and potassium fertilizers; *Y<sub>NP</sub>* denotes the crop yield under the field experiment treatment using nitrogen and phosphorus fertilizers; and *FerN*, *FerP* and *FerK* are the nitrogen, phosphorus and potassium fertilizer rates (kg ha<sup>-1</sup>), respectively, in the fertilizer utilization efficiency field experiment.

$$TFRN = [FIY \times NUTN] / (REN \times 100) \quad (19)$$

$$TFRP = [FIY \times NUTP] / (REP \times 100) \quad (20)$$

$$TFRK = [FIY \times NUTK] / (REK \times 100) \quad (21)$$

$$NBRN = (FRN - TFRN) / TFRN \quad (22)$$

$$NBRP = (FRP - TFRP) / TFRP \quad (23)$$

$$NBRK = (FRK - TFRK) / TFRK \quad (24)$$

where *TFRN*, *TFRP* and *TFRK* denote the theoretical nitrogen fertilizer rate (kg ha<sup>-1</sup>), the theoretical phosphorus fertilizer rate (kg ha<sup>-1</sup>), and the theoretical potassium fertilizer rate (kg ha<sup>-1</sup>) for the crop, respectively; *FRN*, *FRP* and *FRK* denote the actual nitrogen, phosphorus and potassium fertilizer rates (kg ha<sup>-1</sup>) for the crop, respectively; and *NBRN*, *NBRP* and *NBRK* denote the crop nutrient balance ratios (*NBR*) of nitrogen, phosphorus and potassium, respectively (*NBR* > 0 indicates excessive fertilizer inputs; *NBR* = 0 indicates balanced fertilizer inputs; and *NBR* < 0 indicates insufficient fertilizer inputs).

### Multiobjective spatial optimization of crop fertilizer rates

In this study, the NSGA-II was used to optimize crop fertilizer application rates. Step 1: Considering the spatial variability in the crop nutrient balance, the actual fertilizer rate in each grid cell was gradually adjusted to the theoretical fertilizer rate with a gradient of 10% (i.e., the 0% gradient yields the actual fertilizer rate, and the 100% gradient yields the theoretical fertilizer rate), and grid data of nitrogen, phosphorus and potassium fertilizer rates under different adjustment gradients were generated. Step 2: The grid data of all nitrogen fertilizer rate gradients from step 1 were sequentially input into the established RF yield prediction model (with the other model parameters remaining constant) to generate crop nitrogen response yield grid data under different adjustment gradients; the same method was applied to generate crop yield grid data under the predicted phosphorus and potassium fertilizer rate gradients. In step 3, the total nitrogen fertilizer rate (*OFRN*), total phosphorus fertilizer rate (*OFRP*), and total potassium fertilizer rate (*OFRK*) were calculated for the 3 crops under each adjustment gradient in the study area using the fertilizer rate grid data from step 2. The total nitrogen response yield (*OYN*), total phosphorus response yield (*OYP*), and total potassium response yield (*OYK*) were calculated for the 3 crops under each adjustment gradient in the study area using the crop yield grid data from step 2. A linear regression model was fitted with the total crop yield or the total fertilizer rate as the dependent variable and the corresponding adjustment gradient as the independent variable. Step 4: A Pareto solution set was computed via the NSGA module of MATLAB software using the above linear regression model as the objective function. This Pareto solution set contains several preferable solutions, and finally, the combination yielding a stable crop yield (increased or unchanged total yield) and the minimum fertilizer rate (especially nitrogen fertilizer) was selected as the nutrient optimization solution. The objective function can be expressed as:

$$FRN' = TFRN \times [1 + (1 - x_1) \times NBRN] \quad (25)$$

$$FRP' = TFRP \times [1 + (1 - x_2) \times NBRP] \quad (26)$$

$$FRK' = TFRK \times [1 + (1 - x_3) \times NBRK] \quad (27)$$

$$OFRN = \sum_{i=1}^n FRN' \quad (28)$$

$$OFRP = \sum_{i=1}^n FRP' \quad (29)$$

$$OFRK = \sum_{i=1}^n FRK' \quad (30)$$

$$OYN = \sum_{i=1}^n H(FRN') \quad (31)$$

$$OYP = \sum_{i=1}^n H(FRP') \quad (32)$$

$$OYK = \sum_{i=1}^n H(FRK') \quad (33)$$

$$MIN(OFRN) = u(x_1) \quad (34)$$

$$MIN(OFRP) = u(x_2) \quad (35)$$

$$MIN(OFRK) = u(x_3) \quad (36)$$

$$MAX(OYN) = v(x_1) \quad (37)$$

$$MAX(OYP) = v(x_2) \quad (38)$$

$$MAX(OYK) = v(x_3) \quad (39)$$

where  $x_1$ ,  $x_2$  and  $x_3$  denote the adjustment gradients (%) of the nitrogen, phosphorus and potassium fertilizer rates, respectively;  $n$  denotes the total number of grid units for the crop planting map of the study area;  $FRN'$ ,  $FRP'$  and  $FRK'$  denote the nitrogen, phosphorus and potassium fertilizer rates ( $\text{kg ha}^{-1}$ ), respectively, for a given crop in each grid under a certain fertilizer rate adjustment gradient;  $OFRN$ ,  $OFRP$  and  $OFRK$  are the total nitrogen fertilizer rate, total phosphorus fertilizer rate and total potassium fertilizer rate, respectively, for the crop under the fertilizer rate adjustment gradient;  $OYN$ ,  $OYP$  and  $OYK$  denote the total nitrogen response yield, total phosphorus response yield and total potassium response yield, respectively, of the crop under the fertilizer rate adjustment gradient;  $H(x)$  denotes the established RF prediction model for the crop YF;  $u(x_1)$ ,  $u(x_2)$  and  $u(x_3)$  denote the regression models of the adjustment gradients (%) of the nitrogen, phosphorus and potassium fertilizer rates with  $OFRN$ ,  $OFRP$  and  $OFRK$ , respectively; and  $v(x_1)$ ,  $v(x_2)$  and  $v(x_3)$  denote the regression models of the adjustment gradients (%) of the nitrogen, phosphorus and potassium fertilizer rates with  $OYN$ ,  $OYP$  and  $OYK$ , respectively.

In addition, the upper and lower boundary constraints (0–1) were set in MATLAB for parameters  $x_1$ ,  $x_2$ , and  $x_3$ ; the population size was 100; and the number of generations, crossover probability, and mutation probability were set to system default values.

### Data availability

Data is provided within the manuscript or supplementary information files. Full details of all datasets used in the study are further elaborated in the Supplementary Information and available at Dryad (<https://figshare.com/s/bdfac3af64d7cb61b279>). The climate and crop data are publicly available from the Resource and Environmental Science Data Platform (<https://www.resdc.cn>).

### Code availability

No custom codes were generated, but standard packages within ArcGIS (v10.8), Origin (v2021), and SPSS MATLAB (v2023) were used.

Received: 18 April 2025; Accepted: 4 January 2026;

Published online: 02 March 2026

## References

1. Ray, D. K. et al. Crop harvests for direct food use insufficient to meet the UN's food security goal. *Nat. Food* **3**, 367–374 (2022).
2. Huang, Y. et al. Simulating no-tillage effects on crop yield and greenhouse gas emissions in Kentucky corn and soybean cropping systems: 1980–2018. *Agric. Syst.* **197**, 103355 (2022).
3. West, P. C. et al. Leverage points for improving global food security and the environment. *Science* **345**, 325–328 (2014).
4. Gu, B. et al. Cost-effective mitigation of nitrogen pollution from global croplands. *Nature* **613**, 77–84 (2023).
5. Xu, P. et al. Fertilizer management for global ammonia emission reduction. *Nature* **626**, 792–798 (2024).
6. Chang, J. et al. Reconciling regional nitrogen boundaries with global food security. *Nat. Food* **2**, 700–711 (2021).
7. Lanz, B., Dietz, S. & Swanson, T. The Expansion of modern agriculture and global biodiversity decline: an integrated assessment. *Ecol. Econ.* **144**, 260–277 (2018).
8. Richardson, K. et al. Earth beyond six of nine planetary boundaries. *Sci. Adv.* **9**, eadh2458 (2023).
9. Zhang, X. et al. Managing nitrogen for sustainable development. *Nature* **528**, 51–59 (2015).
10. Zou, T., Zhang, X. & Davidson, E. A. Global trends of cropland phosphorus use and sustainability challenges. *Nature* **611**, 81–87 (2022).
11. Prosekov, A. Y. & Ivanova, S. A. Food security: the challenge of the present. *Geoforum* **91**, 73–77 (2018).
12. Qaim, M. Role of new plant breeding technologies for food security and sustainable agricultural development. *Appl. Econ. Perspect. Policy* **42**, 129–150 (2020).
13. Deng, O. et al. Managing fragmented croplands for environmental and economic benefits in China. *Nat. Food* **5**, 230–240 (2024).
14. Folberth, C. et al. The global cropland-sparing potential of high-yield farming. *Nat. Sustain.* **3**, 281–289 (2020).
15. Xie, W. et al. Crop switching can enhance environmental sustainability and farmer incomes in China. *Nature* **616**, 300–305 (2023).
16. Hou, Y. et al. Improving food system sustainability: grid-scale crop layout model considering resource-environment-economy-nutrition. *J. Clean. Prod.* **403**, 136881 (2023).
17. Wang, Z. et al. Integrating crop redistribution and improved management towards meeting China's food demand with lower environmental costs. *Nat. Food* **3**, 1031–1039 (2022).
18. Luna Juncal, M. J., Masino, P., Bertone, E. & Stewart, R. A. Towards nutrient neutrality: a review of agricultural runoff mitigation strategies and the development of a decision-making framework. *Sci. Total Environ.* **874**, 162408 (2023).
19. Smerald, A. et al. A redistribution of nitrogen fertiliser across global croplands can help achieve food security within environmental boundaries. *Commun. Earth Environ.* **4**, 315 (2023).
20. Kahiluoto, H. et al. Redistribution of nitrogen to feed the people on a safer planet. *PNAS nexus* **3**, pgae170 (2024).
21. He, S., Sun, Y. -y, Shen, Z. -q & Wang, K. Advances in coupling big data technique with nutrient site-specific management: scheme, methods and outlook. *J. Plant Nutr. Fertil.* **23**, 1514–1524 (2017).
22. Iizumi, T. et al. Prediction of seasonal climate-induced variations in global food production. *Nat. Clim. Change* **3**, 904–908 (2013).
23. Wang, Y. & Gong, Y. Spectral remote sensing technology applied in crop yield estimation: research progress. *Chin. Agric. Sci. Bull.* **35**, 69–75 (2019).
24. Sun, Y. -y & Shen, S. -H. Research progress in application of crop growth models. *Chin. J. Agrometeorol.* **40**, 444–459 (2019).
25. Mokhtari, A., Noory, H. & Vazifedoust, M. Improving crop yield estimation by assimilating LAI and inputting satellite-based surface

- incoming solar radiation into SWAP model. *Agric. For. Meteorol.* **250**, 159–170 (2018).
26. Chen, S. et al. Weather records from recent years performed better than analogue years when merging with real-time weather measurements for dynamic within-season predictions of rainfed maize yield. *Agric. For. Meteorol.* **315**, 108810 (2022).
  27. Zhou, Q. & Ismaeel, A. Integration of maximum crop response with machine learning regression model to timely estimate crop yield. *Geo-Spat. Inf. Sci.* **24**, 474–483 (2021).
  28. ZHANG, J., FANG, S. & LIU, H. Machine learning approach for estimation of crop yield combining use of optical and microwave remote sensing data. *J. Geo-Inf. Sci.* **23**, 1082–1091 (2021).
  29. Tao, S., Pan, J. & Liu, K. The application progress of DSSAT in field of agriculture and climate change in China. *Chin. Agric. Sci. Bull.* **31**, 200–206 (2015).
  30. de Wit, A. et al. 25 years of the WOFOST cropping systems model. *Agric. Syst.* **168**, 154–167 (2019).
  31. Zhu, Y. et al. Research progress on the crop growth model cropgrow. *Sci. Agric. Sin.* **53**, 3235–3256 (2020).
  32. Zhao, Y. et al. Research progress of APSIM model and its application in China. *Chin. Agric. Sci. Bull.* **33**, 1–6 (2017).
  33. Li, P. et al. Assessment of terrestrial laser scanning and hyperspectral remote sensing for the estimation of rice grain yield. *Sci. Agric. Sin.* **54**, 2965–2976 (2021).
  34. Paudel, D. et al. Machine learning for regional crop yield forecasting in Europe. *Field Crops Res.* **276**, 108377 (2022).
  35. Chang, Y., Latham, J., Licht, M. & Wang, L. A data-driven crop model for maize yield prediction. *Commun. Biol.* **6**, 439 (2023).
  36. Wang, Q., Sun, L. & Yang, X. Identifying spatial determinants of rice yields in main producing areas of China using geospatial machine learning. *ISPRS Int. J. Geo-Inf.* **13**, 76 (2024).
  37. Su, Y. -x, Xu, H. & Yan, L. -j Support vector machine-based open crop model (SBOCM): case of rice production in China. *Saudi J. Biol. Sci.* **24**, 537–547 (2017).
  38. Schwalbert, R. A. et al. Satellite-based soybean yield forecast: integrating machine learning and weather data for improving crop yield prediction in southern Brazil. *Agric. For. Meteorol.* **284**, 107886 (2020).
  39. Xu, H. et al. Machine learning approaches can reduce environmental data requirements for regional yield potential simulation. *Eur. J. Agron.* **129**, 126335 (2021).
  40. Gómez, D., Salvador, P., Sanz, J. & Casanova, J. L. Modelling wheat yield with antecedent information, satellite and climate data using machine learning methods in Mexico. *Agric. For. Meteorol.* **300**, 108317 (2021).
  41. van Grinsven, H. J. M. et al. Establishing long-term nitrogen response of global cereals to assess sustainable fertilizer rates. *Nat. Food* **3**, 122–132 (2022).
  42. Van Klompenburg, T., Kassahun, A. & Catal, C. Crop yield prediction using machine learning: a systematic literature review. *Comput. Electron. Agric.* **177**, 105709 (2020).
  43. Jeong, J. H. et al. Random forests for global and regional crop yield predictions. *PLoS ONE* **11**, e0156571 (2016).
  44. Li, L. et al. Integrating machine learning and environmental variables to constrain uncertainty in crop yield change projections under climate change. *Eur. J. Agron.* **149**, 126917 (2023).
  45. Liu, X., Zhang, D., Wu, H., Elser, J. J. & Yuan, Z. Uncovering the spatio-temporal dynamics of crop-specific nutrient budgets in China. *J. Environ. Manag.* **340**, 117904 (2023).
  46. Vitousek, P. M. et al. Nutrient imbalances in agricultural development. *Science* **324**, 1519–1520 (2009).
  47. Zhang, X. et al. Quantifying nutrient budgets for sustainable nutrient management. *Glob. Biogeochem. Cycles* **34**, e2018GB006060 (2020).
  48. Carmo, M., García-Ruiz, R., Ferreira, M. I. & Domingos, T. The N-P-K soil nutrient balance of Portuguese cropland in the 1950s: the transition from organic to chemical fertilization. *Sci. Rep.* **7**, 8111 (2017).
  49. Koritschoner, J. J., Whitworth Hulse, J. I., Cuchietti, A. & Arrieta, E. M. Spatial patterns of nutrients balance of major crops in Argentina. *Sci. Total Environ.* **858**, 159863 (2023).
  50. Bassanino, M., Sacco, D., Zavattaro, L. & Grignani, C. Nutrient balance as a sustainability indicator of different agro-environments in Italy. *Ecol. Indic.* **11**, 715–723 (2011).
  51. Spiess, E. Nitrogen, phosphorus and potassium balances and cycles of Swiss agriculture from 1975 to 2008. *Nutr. Cycl. Agroecosyst.* **91**, 351–365 (2011).
  52. Jiang, Q. Analysis of temporal and spatial variations of nutrient balance and its environmental risk in Zhejiang province. *Resour. Environ. Yangtze Basin* **27**, 295 (2018).
  53. Guo, L., Yang, R. & Wang, D. A study on the spatial difference of farmland nitrogen nutrient budget in the Bohai Rim region, China. *J. Geogr. Sci.* **22**, 761–768 (2012).
  54. Yang, D. Characteristics of nitrogen balance model and pollution risk assessment in Yangtze River economic zone. *Ecol. Environ.* **29**, 1344–1351 (2020).
  55. Shu-Tian, L. Characteristics of nutrient input/output and nutrient balance in different regions of China. *Sci. Agric. Sin.* **44**, 4207–4229 (2011).
  56. Hong, X. -y. et al. Nutrient balance in farmlands and the resulting environmental risk in Hainan Province. *J. Plant Nutr. Fertil.* **28**, 2070–2081 (2022).
  57. Mishima, S. -I., Kimura, S. D., Eguchi, S. & Shirato, Y. Changes in soil available-nutrient stores and relationships with nutrient balance and crop productivity in Japan. *Soil Sci. Plant Nutr.* **59**, 371–379 (2013).
  58. Liu, Y. et al. Temporal and spatial variation of potassium balance in agricultural land at national and regional levels in China. *PLoS ONE* **12**, e0184156 (2017).
  59. Zheng, L. et al. Nitrogen and phosphorus trajectories (1998–2030) under regional development strategy of mainland China. *Sci. Total Environ.* **794**, 148655 (2021).
  60. van Leeuwen, M. M. W. J. et al. The relevance of spatial scales in nutrient balances on dairy farms. *Agri. Ecosyst. Environ.* **269**, 125–139 (2019).
  61. Cui, Z. Soil nutrient balance in rice–wheat rotation system in Taizhou City of Jiangsu Province. *J. Plant Nutr. Fertil.* **25**, 1002–1009 (2019).
  62. XiaoYan, M. Annual nutrients balance and economic return analysis of wheat with fertilizers reduction and different rotations. *Sci. Agric. Sin.* **55**, 1589–1603 (2022).
  63. Ren, D. et al. Modeling and assessing water and nutrient balances in a tile-drained agricultural watershed in the U.S. Corn Belt. *Water Res.* **210**, 117976 (2022).
  64. Yang, J. Y. et al. Simulating nitrogen balance in Canadian agricultural soils from 1981 to 2016. *J. Environ. Manag.* **341**, 118015 (2023).
  65. Bao, Y. -I. et al. Review on site-specific management zone for zonal fertilization delineation in last 20 years. *Chin. J. Soil Sci.* **52**, 988–999 (2021).
  66. Yao, R. -J. et al. Determination of site-specific management zones using soil physico-chemical properties and crop yields in coastal reclaimed farmland. *Geoderma* **232–234**, 381–393 (2014).
  67. Shaddad, S. M., Madrau, S., Castrignanò, A. & Mouazen, A. M. Data fusion techniques for delineation of site-specific management zones in a field in UK. *Precis. Agric.* **17**, 200–217 (2016).
  68. Farid, H. U., Bakhsh, A., Ahmad, N., Ahmad, A. & Mahmood-Khan, Z. Delineating site-specific management zones for precision agriculture. *J. Agric. Sci.* **154**, 273–286 (2016).

69. Ali, A. M. & Ibrahim, S. M. Establishment of soil management zones using multivariate analysis and GIS. *Commun. Soil Sci. Plant Anal.* **51**, 2491–2500 (2020).
70. Abdel-Fattah, M. K. A GIS-based approach to identify the spatial variability of salt affected soil properties and delineation of site-specific management zones: a case study from Egypt. *Soil Sci. Ann.* **71**, 76–85 (2020).
71. Huang, Q., Dang, H., Huang, T., Hou, S. & Wang, Z. Evaluation of farmers' fertilizer application and fertilizer reduction potentials in major wheat production regions of China. *Sci. Agric. Sin.* **53**, 4816–4834 (2020).
72. Yang, Y.-M., Huang, S.-H., Yang, J.-f. & Jia, L.-I. Analysis of wheat fertilizer reduction potential in Hebei province. *Soil Fertil. Sci. China* **36**, 1481 (2021).
73. McDowell, R. W., Pletnyakov, P. & Haygarth, P. M. Phosphorus applications adjusted to optimal crop yields can help sustain global phosphorus reserves. *Nat. Food* **5**, 332–339 (2024).
74. Siatwiinda, S. M., Ros, G. H., Yerokun, O. A. & de Vries, W. Options to reduce ranges in critical soil nutrient levels used in fertilizer recommendations by accounting for site conditions and methodology: a review. *Agron. Sustain. Dev.* **44**, 9 (2024).
75. Xiao, L. et al. Spatiotemporal co-optimization of agricultural management practices towards climate-smart crop production. *Nat. Food* **5**, 59–71 (2024).
76. Bai, Z. et al. Optimizing phosphorus fertilizer use to enhance water quality, food security and social equality. *Resour. Conserv. Recycl.* **203**, 107400 (2024).
77. Gao, P., Wang, H., Song, C., Cheng, C. & Shen, S. NSGA multi-objective optimization algorithms and geographic decision-making: principles, state of the art, and the future. *J. Geo-Inf. Sci.* **25**, 25–39 (2023).
78. Wang, Q., Liu, R., Men, C. & Guo, L. Application of genetic algorithm to land use optimization for non-point source pollution control based on CLUE-S and SWAT. *J. Hydrol.* **560**, 86–96 (2018).
79. Wang, L. et al. Optimization of the planting structure in the upstream region of Baiyangdian Lake based on the non-dominated sorting genetic algorithm (NSGA-II). *Chin. J. Eco-Agric.* **29**, 1370–1383 (2021).
80. Wu, X., Pan, J. & Zhu, X. Optimizing the ecological source area identification method and building ecological corridor using a genetic algorithm: a case study in Weihe River Basin, NW China. *Ecol. Inform.* **80**, 102519 (2024).
81. Gerber, J. S. et al. Global spatially explicit yield gap time trends reveal regions at risk of future crop yield stagnation. *Nat. Food* **5**, 125–135 (2024).
82. Hu, Y. et al. Food production in China requires intensified measures to be consistent with national and provincial environmental boundaries. *Nat. Food* **1**, 572–582 (2020).
83. Wang, A., Yang, D. & Tang, L. Spatiotemporal variation in nitrogen loads and their impacts on river water quality in the upper Yangtze River basin. *J. Hydrol.* **590**, 125487 (2020).
84. Liu, G., Zhang, F. & Deng, X. Half of the greenhouse gas emissions from China's food system occur during food production. *Commun. Earth Environ.* **4**, 161 (2023).
85. Chen, S., Lin, B., Li, Y. & Zhou, S. Spatial and temporal changes of soil properties and soil fertility evaluation in a large grain-production area of subtropical plain, China. *Geoderma* **357**, 113937 (2020).
86. Guo, J., Li, C., Xu, X., Sun, M. & Zhang, L. Farmland scale and chemical fertilizer use in rural China: new evidence from the perspective of nutrient elements. *J. Clean. Prod.* **376**, 134278 (2022).
87. Tan, S. et al. Characteristics and influencing factors of chemical fertilizer and pesticide applications by farmers in hilly and mountainous areas of Southwest, China. *Ecol. Indic.* **143**, 109346 (2022).
88. Chuan, L.-M., He, P. & Zhao, T.-K. Research advance on recommendation for crop fertilization methodology. *J. Agric. Sci. Technol.* **18**, 95–102 (2016).
89. Zhang, M., Li, J., Kong, Q. & Yan, F. Progress and prospect of the study on crop-response-to-fertilization function model. *Acta Pedol. Sin.* **53**, 1343–1356 (2016).
90. Xu, Y. et al. Progress and prospects for the project of formula fertilization by soil testing in the last 15 years. *Soil Fertil. Sci. China* **3**, 236–244 (2023).
91. Zhou, W. & Ding, W. -c Strategic researches of reducing fertilizer use and increasing use efficiency in China in the new era. *J. Plant Nutr. Fertil.* **29**, 1–7 (2023).
92. O'Connell, C. & Osmond, D. L. Why soil testing is not enough: a mixed methods study of farmer nutrient management decision-making among U.S. producers. *J. Environ. Manag.* **314**, 115027 (2022).
93. Li, J., Zhang, M., Xu, W., Kong, Q. & Yao, B. Principal component regression technology of ternary fertilizer response model for improving success rate of modeling. *Acta Pedol. Sin.* **55**, 467–478 (2018).
94. Folberth, C. et al. Uncertainty in soil data can outweigh climate impact signals in global crop yield simulations. *Nat. Commun.* **7**, 11872 (2016).
95. Wang, Q. et al. Spatial and temporal variation characteristics of the main agricultural inputs in Sichuan Province and the influencing factors. *J. Ecol. Rural Environ.* **34**, 717–725 (2018).
96. Sichuan Provincial Department of Agriculture and Rural Affairs. *Guidance on Scientific Fertilization for Major Crops in Sichuan Province, 2021–2025*, <http://nynct.sc.gov.cn/nynct/qtwj/2021/2/10/e49bc1a6331642e196197503944557c6.shtml> (2021).
97. Liang, T. et al. Response of rice yield to inherent soil productivity of paddies and fertilization in Sichuan Basin. *Sci. Agric. Sin.* **48**, 4759–4768 (2015).
98. Xu, C. et al. The response of maize yield to inherent soil productivity and fertilizer in the Southwest. *Sci. Agric. Sin.* **51**, 129–138 (2018).
99. Zheng, S. et al. Responses of rice yields to basic soil fertility and fertilization in Western Sichuan Plain. *J. China Agric. Univ.* **23**, 8 (2018).
100. Liu, H.-B., Gou, Y., Wang, H.-Y., Li, H.-M. & Wu, W. Temporal changes in climatic variables and their impact on crop yields in southwestern China. *Int. J. Biometeorol.* **58**, 1021–1030 (2014).
101. Baloch, N. et al. Effect of latitude on maize kernel weight and grain yield across China. *Agron. J.* **113**, 1172–1182 (2021).
102. Liu, Y. et al. Comprehensive assessment of “climate change–crop yield–economic impact” in seven sub-regions of China. *Adv. Clim. Change Res.* **17**, 455–465 (2021).
103. Ringeval, B. et al. Limitation of maize potential yield by phosphorus at the global scale. *Glob. Change Biol.* **31**, e70485 (2025).
104. Sun, S., Zhang, L., Chen, Z. & Sun, J. Advances in aquacrop model research and application. *Sci. Agric. Sin.* **50**, 3286–3299 (2017).
105. Wang, T., Yuan, S. & Wang, J. Study on vulnerability of drought hazard affected rice in Sichuan Province. *J. Nat. Disaster.* **22**, 221–226 (2013).
106. Deutsch, C. A. et al. Increase in crop losses to insect pests in a warming climate. *Science* **361**, 916–919 (2018).
107. LI, S.-T. & Jin, J.-Y. Characteristics of nutrient input/output and nutrient balance in different regions of China. *Sci. Agric. Sin.* **44**, 4207–4229 (2011).
108. Zhang, Z. et al. Effects of nitrogen fertilization on rice in different regions of Sichuan Province. *Acta Pedol. Sin.* **52**, 234–241 (2015).
109. Chen, S.-h. et al. Current status and evaluation of nutrient management for maize in southwest China. *Soil Fertil. Sci. China* **1**, 159–165 (2019).

110. Zhang, W. et al. Re-prediction of phosphate fertilizer demand in China based on agriculture green development. *Acta Pedol. Sin.* **60**, 1389–1397 (2023).
111. Chen, D. et al. Spatial variation characteristics and influencing factors of soil available phosphorus in cultivated land in the Sichuan Basin. *J. Plant Nutr. Fertil.* **30**, 1768–1781 (2024).
112. Brownlie, W. J. et al. Global food security threatened by potassium neglect. *Nat. Food* **5**, 111–115 (2024).
113. Ji, H., Zhang, H., Zhang, W. & Tian, C. Farmland potassium balance in China: a review. *Chin. J. Eco-Agric.* **25**, 920–930 (2017).
114. ZHANG, W. -j, WANG, C. -q, YUAN, D. -g, LI, B. & ZHANG, W. -y Status, problems and countermeasures of main crops' fertilizer application in sichuan province. *Chin. J. Soil Sci.* **45**, 697–703 (2014).
115. Cai, S. et al. Optimal nitrogen rate strategy for sustainable rice production in China. *Nature* **615**, 73–79 (2023).
116. Li, B., Yan, L. & Zhang, W. Study on N application and N reduction potential of farmland in China. *Environ. Monit. Assess.* **195**, 1156 (2023).
117. Dong, Y.-j., Yuan, J., Mu, W. & Lyu, S.-h. Preliminary study on potential of stable yield and nitrogen reduction in paddy-upland rotation system in Chengdu Plain. *Southwest China J. Agric. Sci.* **34**, 2437–2444 (2021).
118. Liao, G. et al. Nutrient use efficiency has decreased in southwest China since 2009 with increasing risk of nutrient excess. *Commun. Earth Environ.* **4**, 388 (2023).
119. Wu, L., Wu, L., Cui, Z., Chen, X. & Zhang, F. Basic NPK fertilizer recommendation and fertilizer formula for maize production regions in China. *Acta Pedol. Sin.* **52**, 802–817 (2015).
120. Wu, L.-Q., WU, L., Cui, Z. -l, Chen, X. -p & Zhang, F. -s Studies on recommended nitrogen, phosphorus and potassium application rates and special fertilizer formulae for different rice production regions in China. *J. China Agric. Univ.* **21**, 1–13 (2016).
121. Sun, Y. -x et al. Establishing phosphorus and potassium fertilization recommendation index based on the '3414' field experiments. *J. Plant Nutr. Fertil.* **15**, 197–203 (2009).
122. Hou, M. et al. Concurrent drought threatens wheat and maize production and will widen crop yield gaps in the future. *Agric. Syst.* **220**, 104056 (2024).
123. Cai, Z. Scientific and technological issues of nutrient management under greenhouse cultivation in China. *Acta Pedol. Sin.* **56**, 36–43 (2019).
124. Ministry of Agriculture and Rural Affairs of the People's Republic of China. *Action Plan for Reducing Chemical Fertilizer Use by 2025*, [https://www.moa.gov.cn/govpublic/ZZYGLS/202212/t20221201\\_6416398.htm](https://www.moa.gov.cn/govpublic/ZZYGLS/202212/t20221201_6416398.htm) (2022).
125. Sichuan Statistics Bureau. *Sichuan Yearbook (2020)*. (University of Electronic Science and Technology of China Press, 2020).
126. Sichuan Statistics Bureau. *Sichuan Statistical Yearbook (2009)*. (China Statistics Press, 2009).
127. Tian, R. et al. Environmental risk assessment and trend simulation of non-point source pollution of chemical fertilization in Sichuan Province, China. *Chin. J. Eco-Agric.* **26**, 1739 (2018).
128. Shen, R. et al. High-resolution distribution maps of single-season rice in China from 2017 to 2022. *Earth Syst. Sci. Data* **15**, 3203–3222 (2023).
129. Dong, J. et al. Early-season mapping of winter wheat in China based on Landsat and Sentinel images. *Earth Syst. Sci. Data* **12**, 3081–3095 (2020).
130. Shen, R. et al. A 30 m resolution distribution map of maize for China based on Landsat and Sentinel images. *J. Remote Sens.* **2022**, 9846712 (2022).
131. Goovaerts, P. Geostatistics in soil science: state-of-the-art and perspectives. *Geoderma* **89**, 1–45 (1999).
132. liu, Q.-X. et al. Analysis of spatial distribution and influencing factors of nitrogen and phosphorus fertilizer application intensity in Chengdu plain. *Environ. Sci.* **42**, 3556–3565 (2021).
133. Xu, X. China GDP spatial distribution kilometer grid dataset. *Data Registration and Publishing System of the Resource and Environmental Science Data Center of the Chinese Academy of Sciences* (<http://www.resdc.cn/DOI>), <https://doi.org/10.12078/2017121102> (2017).
134. Xu, X. China's population spatial distribution kilometer grid dataset. *Data Registration and Publishing System of the Resource and Environmental Science Data Center of the Chinese Academy of Sciences* (<http://www.resdc.cn/DOI>), <https://doi.org/10.12078/2017121101> (2017).
135. Xu, X. China Annual Vegetation Index (NDVI) spatial distribution dataset. *Data Registration and Publishing System of the Resource and Environmental Science Data Center of the Chinese Academy of Sciences* (<http://www.resdc.cn/DOI>), <https://doi.org/10.12078/2018060601> (2018).
136. Xu, X., Liu, L. & Cai, H. China's Farmland Production Potential Data Set. *Data Registration and Publishing System of the Resource and Environmental Science Data Center of the Chinese Academy of Sciences* (<http://www.resdc.cn/DOI>), <https://doi.org/10.12078/2017122301> (2017).
137. Sichuan Statistics Bureau. *Sichuan Statistical Yearbook (2020)*. (China Statistics Press, 2020).
138. Breiman, L. Random forests. *Mach. Learn.* **45**, 5–32 (2001).
139. Zou, Y. -b, Xia, B., Jiang, P., Xie, X. -b & Huang, M. Discussion on the theory and methods for determining the target yield in rice production. *Sci. Agric. Sin.* **48**, 4021–4032 (2015).
140. liao, Y. -l et al. Effects of long-term fertilization on basic soil productivity and nutrient use efficiency in paddy soils. *J. Plant Nutr. Fertil.* **22**, 1249–1258 (2016).
141. Deng, X., Deng, J., Wang, L., Gong, X. & Li, T. Effects of NPK fertilizers combined on agronomic traits, yield, nutrient uptake and utilization of "Heyu 9566. *Maize Crops* **32**, 156–161 (2016).
142. Zhao, H., Zhao, X., Xie, L. & Guo, X. Spatial variation and its affecting factors of rice fertilizer use efficiency in Shangrao City of Jiangxi Province. *Acta Pedol. Sin.* **51**, 21–31 (2014).
143. Zhang, F. et al. Nutrient use efficiencies of major cereal crops in China and measures for improvement. *ACTA Pedol. Sin.* **45**, 915–924 (2008).
144. Shao, H., Zhu, A., Shi, Q. & Zhao, X. Study on the recommended nitrogen fertilization system of rice in Jiangxi province. *Soil Fertil. Sci. China.* **5**, 55–60 (2016).
145. Liu, X. & Li, S. Temporal and spatial distribution characteristics of crop straw nutrient resources and returning to farmland in China. *Trans. Chin. Soc. Agric. Eng.* **33**, 1–19 (2017).

### Acknowledgements

This work was financially supported by the Yibin Agricultural Science and Technology Innovation Project (2024NYHZ005), the Independent Innovation Project of the Sichuan Academy of Agricultural Sciences (2022ZZCX036), the Key Research and Development Project of Sichuan Province (2021YFYZ0028), the Special Funds for the Sichuan Pepper Innovation Team of the Modern Agricultural Industry Technology System (SCCXTD-2024-23), and Chengdu University of Information Technology (KYTZ202116). We would like to thank the anonymous reviewers for their valuable comments and suggestions.

### Author contributions

G.T.L. and X.G. conceived and led the project. G.T.L., P.H., and X.G. designed the experiments and methodology. J.M.Q. contributed data and analysed the field experimental data. P.H. and Z.Y.L. contributed data and produced the maps. T.F.D. and G.H. contributed data and analysed the soil data. C.H.X. revised the manuscript. G.T.L. wrote and revised the manuscript. All authors discussed the results and implications and commented on the manuscript at all stages.

### Competing interests

The authors declare no competing interests.

### Additional information

**Supplementary information** The online version contains supplementary material available at

<https://doi.org/10.1038/s44264-026-00127-y>.

**Correspondence** and requests for materials should be addressed to Guitang Liao or Xi Gou.

**Reprints and permissions information** is available at <http://www.nature.com/reprints>

**Publisher's note** Springer Nature remains neutral with regard to jurisdictional claims in published maps and institutional affiliations.

**Open Access** This article is licensed under a Creative Commons Attribution-NonCommercial-NoDerivatives 4.0 International License, which permits any non-commercial use, sharing, distribution and reproduction in any medium or format, as long as you give appropriate credit to the original author(s) and the source, provide a link to the Creative Commons licence, and indicate if you modified the licensed material. You do not have permission under this licence to share adapted material derived from this article or parts of it. The images or other third party material in this article are included in the article's Creative Commons licence, unless indicated otherwise in a credit line to the material. If material is not included in the article's Creative Commons licence and your intended use is not permitted by statutory regulation or exceeds the permitted use, you will need to obtain permission directly from the copyright holder. To view a copy of this licence, visit <http://creativecommons.org/licenses/by-nc-nd/4.0/>.

© The Author(s) 2026